Quaternary Geochronology 68 (2022) 101244

Contents lists available at ScienceDirect

Quaternary Geochronology

journal homepage: www.elsevier.com/locate/quageo

Revised ΔR values for the Barents Sea and its archipelagos as a pre-requisite for accurate and robust marine-based ^{14}C chronologies

Anna J. Pieńkowski [a,*,1], Katrine Husum [a], Mark F.A. Furze [b], Amandine F.J.M. Missana [b,c], Nil Irvalı [d], Dmitry V. Divine [a], Vårin Trælvik Eilertsen [e]

[a] Norwegian Polar Institute, Fram Centre, N-9296, Tromsø, Norway
[b] Department of Arctic Geology, UNIS (University Centre in Svalbard), N-9171, Longearbyen, Svalbard, Norway
[c] Department of Physical Geography, Stockholm University, SE-106 91, Stockholm, Sweden
[d] Department of Earth Science and Bjerknes Centre for Climate Research, University of Bergen, N-5007, Bergen, Norway
[e] Department of Geosciences, UiT the Arctic University of Norway, N-9037, Tromsø, Norway

ARTICLE INFO

Keywords:
Reservoir correction
Calibration
Arctic
Radiocarbon
Molluscs
Cetaceans

ABSTRACT

The calibration of marine ^{14}C dates requires the incorporation of regionally specific marine reservoir offsets known as ΔR, essential for accurate and meaningful inter-archive comparisons. Revised, regional ΔR ('ΔR_R') values for the Barents Sea are presented for molluscs and cetaceans for the two latest iterations of the marine calibration curve, based on previously published pre-bomb live-collected and radiocarbon-dated samples ('ΔR_L'; molluscs: n = 16; cetaceans: n = 18). Molluscan ΔR_R, determined for four broad regional oceanographic settings, are: western Svalbard (including Bjørnøya), −61 ± 37 ^{14}C yrs (Marine20), 94 ± 38 ^{14}C yrs (Marine13); Franz Josef Land, −277 ± 57 ^{14}C yrs (Marine20), −122 ± 38 ^{14}C yrs (Marine13); Novaya Zemlya, −156 ± 73 ^{14}C yrs (Marine20), 0 ± 76 ^{14}C yrs (Marine13); northern Norway, −86 ± 39 ^{14}C yrs (Marine20), 74 ± 24 ^{14}C yrs (Marine13). Molluscan ΔR_R values are considered applicable to other marine carbonate materials (e.g., foraminifera, ostracods). Cetacean ΔR_R are determined for toothed (n = 10) and baleen (n = 8) whales, and a combined toothed-baleen group (n = 18): toothed, −161 ± 41 ^{14}C yrs (Marine20), 1 ± 41 ^{14}C yrs (Marine13); baleen, −158 ± 43 ^{14}C yrs (Marine20), 8 ± 41 ^{14}C yrs (Marine13); combined baleen-toothed whales, −160 ± 41 ^{14}C yrs (Marine20), 4 ± 49 ^{14}C yrs (Marine13). Where identification and separation of baleen and toothed whales is impossible the combined ΔR_R term may be used. However, we explicitly discourage the application of existing cetacean ΔR_R terms to other marine mammals. Our new ΔR_R values are applicable for as long as those broad oceanographic conditions (circulation and ventilation) have persisted, i.e., through the Holocene. We recommend using the latest iteration of the marine calibration curve, Marine20, which seems to better capture the time-variant nature of R compared to Marine13. More ΔR_L datapoints for both molluscs and cetaceans would improve the accuracy and precision of ΔR_R. In the meantime, our new ΔR terms facilitate the calibration of marine ^{14}C dates across the region, paving the way for meaningful and accurate late Quaternary histories and inter-regional comparisons.

1. Introduction

The uptake of radiocarbon by the ocean lags behind that of the terrestrial ^{14}C reservoir due to the comparatively slow nature of the global marine circulation. Therefore, a global marine-terrestrial offset (known as 'R') needs to be incorporated when converting marine radiocarbon dates into calendar-equivalent ages. This global average marine reservoir age R amounts to ~400–600 years, meaning that marine radiocarbon ages appear several hundred years older compared to contemporaneous terrestrial ones. Importantly, R has fluctuated through time according to atmospheric ^{14}C production and varying ocean circulation and ventilation (Stuiver and Braziunas, 1985). These temporal (annual) fluctuations in global ocean ^{14}C have been modelled (Reimer et al., 2013; Heaton et al., 2020), in contrast to the long-term annual terrestrial ^{14}C variability directly derived from Holocene tree ring data (e.g., Reimer et al., 2013). Marine radiocarbon dates can

* Corresponding author.
E-mail address: Anna.Pienkowski@npolar.no (A.J. Pieńkowski).
[1] Current address: Institute of Geology, Adam Mickiewicz University, 61–606 Poznań, Poland.

https://doi.org/10.1016/j.quageo.2021.101244
Received 5 July 2021; Received in revised form 27 October 2021; Accepted 3 November 2021
Available online 10 November 2021

readily be converted into calendar-equivalent ages in calibration programs (e.g., Calib, OxCal) by selecting the marine radiocarbon curve, which incorporates R and its time-variant nature. However, the calibration of marine dates requires an additional correction because the apparent ages of marine samples are also influenced by local factors that determine the degree of ventilation, i.e., the exchange of carbon between the atmosphere and the ocean influenced by factors including sea-ice cover, upwelling, and freshwater inflow (associated with terrestrial carbon influx), amongst others. This additional offset, known as ΔR, is defined as the difference between the age of the local marine reservoir and the modelled age of the global ocean surface mixed layer (Stuiver et al., 1986). Although ΔR will therefore vary on an individual and local scale ('ΔR_L') according to the local oceanography and degree of ventilation, its spatial variability can be described statistically as a regional offset ('ΔR_R') within an oceanographically defined area (e.g., Eiriksson et al., 2004, 2011; Ulm, 2006; Petchey et al., 2008; Coulthard et al., 2010), remaining approximately the same within a similar oceanographic setting. Unfortunately, a straightforward determination of modern ΔR_R is prevented by the impact of atomic-bomb-derived ^{14}C on the ocean reservoir after 1956 (e.g., Druffel, 1997; Hua et al., 2005). Practically, determining ΔR_R necessitates the use of pre-bomb live--collected dateable marine material such as molluscs or co-occurring contemporaneous terrestrial and marine materials (Alves et al., 2018).

Calibrating marine dates that incorporate an appropriate ΔR_R is a prerequisite for accurate and meaningful comparisons between climatic reconstructions derived from marine and terrestrial archives, both regionally and globally, and between chronologies derived by ^{14}C and other methods. Such an approach is especially pertinent in archipelago settings such as Arctic Canada or Svalbard, where marine and terrestrial environments are tightly interconnected, and where late Quaternary histories have considerable marine- and nearshore-derived components (e.g., Elverhøi et al., 1998; England et al., 2009; Farnsworth et al., 2020). The dynamic interaction between Atlantic and Arctic oceans in the Barents Sea (Fig. 1) makes this region particularly sensitive to climatic and oceanographic change, both past and present (Smedsrud et al., 2013). Accurate Quaternary histories from this area are therefore fundamental to our understanding of the environmental evolution of the Arctic overall, as well as being highly informative to how the circumpolar North will respond to ongoing and future climate change, with parallels for the future found in the past (e.g., the Holocene Thermal Maximum, Pieńkowski et al., 2021).

Despite this importance, only limited data for ΔR calculations are available from the Barents Sea region, with the last published values generated for the Marine04 curve (Mangerud et al., 2006). There have been no subsequent updates for the last 15 years, a period that has seen three new iterations of the marine radiocarbon curve (Reimer et al., 2009, 2013; Heaton et al., 2020) and considerable research efforts across this area (Farnsworth et al., 2020). Here, we present new, regionally-specific marine reservoir offset (ΔR) values for the Svalbard – Barents Sea region (Fig. 1), calculated from previously published pre-bomb collected and radiocarbon dated molluscan materials. We calculate ΔR values and provide recommendations for the use of appropriate ΔR in the calibration of marine radiocarbon dates into calendar-equivalent ages. Terms are presented for both Marine13 (Reimer et al., 2013) and Marine20 (Heaton et al., 2020) to explore differences in the two latest iterations of the marine calibration curve, since the global average marine reservoir age (R) has increased by approximately 1.5 times in Marine20 compared to earlier curves. We further provide guidance on appropriate ΔR values for baleen and toothed whales. Our new ΔR terms will facilitate the calibration of

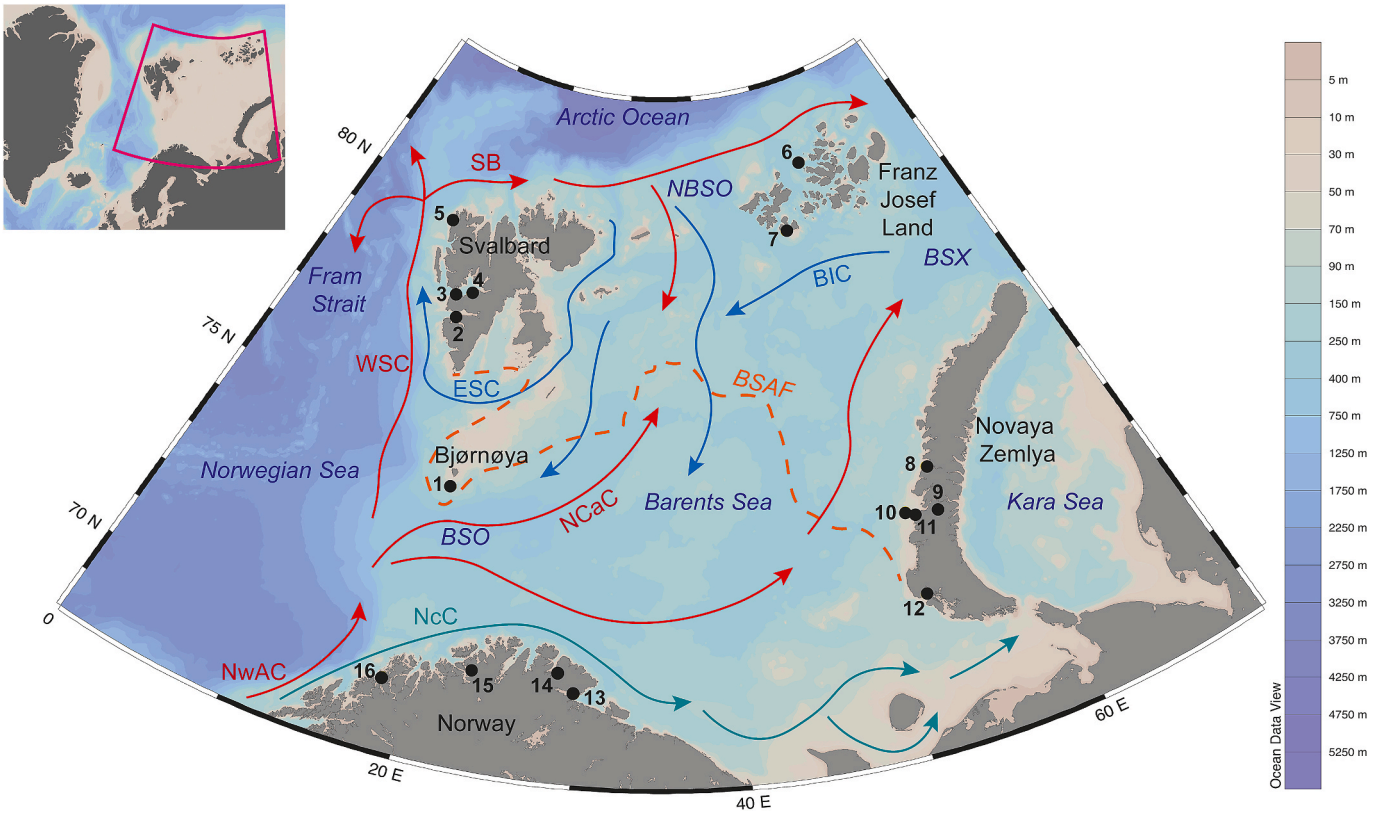

Fig. 1. Map of the Barents Sea, showing bathymetry, general oceanographic circulation (cold and warm currents denoted in blue and red colours, respectively), and oceanographic features. Sites of available pre-bomb collected and radiocarbon dated molluscs are denoted by black circles, with numbers corresponding to site details in Table 1. The base map was drawn in Ocean Data View (Schlitzer, 2020). Abbreviations: BIC, Bear Island Current; BSAF, Barents Sea Arctic Front; BSO, Barents Sea Opening; BSX, Barents Sea Exit; ESC, East Spitsbergen Current; NBSO, Northern Barents Sea Opening; NcC, Norwegian Coastal Current; NCaC, North Cape Current; NwAC, Norwegian Atlantic Current; SB, Svalbard Branch; WSC, West Spitsbergen Current.

marine ^{14}C dates across the region, paving the way for meaningful and accurate late Quaternary histories and inter-regional comparisons.

2. Regional setting

The Barents Sea is a key region for oceanic interaction (Fig. 1) and water mass transformation in the Northern hemisphere, particularly as a gateway for Atlantic water input into the Arctic Ocean and as an area of dynamic atmosphere-ice-ocean heat exchange (Vinje 2001; Beszyńska-Möller et al., 2011; Smedsrud et al., 2013). Its modern oceanography is marked by an interaction between waters sourced from the Atlantic and Arctic oceans, influenced by a relatively shallow continental shelf (average depth 230 m) and seasonal sea-ice formation (Gammelsrød et al., 2009; Ingvaldsen and Loeng, 2009; Smedsrud et al., 2013).

The region west and north of Svalbard is heavily influenced by the West-Spitsbergen Current (WSC; Fig. 1), derived from a branch of the Norwegian Atlantic Current (NwAC), which flows northward from the Norwegian coast, continuing along the continental slope as a surface current (Smedsrud et al., 2013). The Barents Sea Opening (BSO) is where the NwAC splits into the WSC and the North Cape Current (NCaC) which continues into the central Barents Sea. The WSC represents the main input of Atlantic Water into the Arctic Ocean via Fram Strait between Svalbard and Greenland (Beszynska-Möller et al., 2011). Northwest of Svalbard the WSC divides into three branches, one of which (SB, the Svalbard Branch) flows along the northern Svalbard margin and the southern edge of the Nansen Basin of the Arctic Ocean. The SB loops back southward flowing through the North Barents Sea Opening (NBSO) situated between Svalbard and Franz Josef Land (Fig. 1). The NBSO also receives cold Polar Water from the Arctic Ocean which transforms into Arctic Water *en route*, winding its way southwestward as the Eastern Svalbard Current (ESC) and flowing around the southern and western coast of Spitsbergen. An outflow of Arctic Water is additionally found between Franz Josef Land and Novaya Zemlya (St. Anna Trough) through the Barents Sea Exit (BSX) where the Bear Island Current (BIC) flows southwestward (Smedsrud et al., 2013). A strong influence of Arctic Water characterizes the area between Svalbard, Franz Josef Land, and Novaya Zemlya (Fig. 1), whereas the immediate vicinity east of the Svalbard archipelago is somewhat more complicated. There, the dynamic interaction between waters of Atlantic, Polar, and Arctic origins (Fig. 1) challenges straightforward determination of ΔR_R, the consequences of which we elaborate on in the Discussion. The Barents Sea Arctic Front (BSAF; see below) effectively divides the Barents Sea into a northern sector dominated by surface water sourced from the Arctic Ocean and a southern, Atlantic-influenced part, with additional Atlantic Water continuing along the western and northern Svalbard margin as the SB (Loeng, 1991; Ingvaldsen and Loeng, 2009; Smedsrud et al., 2013). The region south of the BSAF is affected by the other branch of the NwAC, the NCaC, which flows into the Barents Sea via the BSO in Bjørnøya Trough.

The oceanography outlined above illustrates the dynamic setting of the Barents Sea under both Atlantic and Arctic water influence (Ingvaldsen and Loeng, 2009). Accordingly, water mass endmembers are the warm and saline Atlantic Water (temperature $\geq$3.5 °C, salinity >35) and cold and fresher Arctic Water (now also referred to as Polar Water, <0 °C, 34–34.9; Sundfjord et al., 2020). Other, locally formed water masses occur in the region as a result of mixing, solar heating, and sea ice formation and melt (Loeng, 1991; Ozhigin et al., 2000; Sundfjord et al., 2020).

Several biologically important front systems are found in the Barents Sea (Fig. 1; e.g., Loeng et al., 1991; Parsons et al., 1996; Pfirman et al., 1994). West of Svalbard, the meeting of the WSC flowing along the continental shelf and the fresher and colder Arctic Water on the continental shelf in the ESC produces the Arctic Front (also referred to as Polar Ocean Front, Nordic Seas Arctic Front, or Polar Front). South- and southeastward of Svalbard the meeting of Atlantic and Arctic waters forms the Barents Sea Arctic Front (BSAF; also called the Polar Front or Barents Sea Polar Front), which is a continuation of the Arctic Front (Pfirman et al., 1994). The BSAF is strongly controlled by topography, especially in the west around Bjørnøya Trough, as well as the strength of Atlantic Water inflow via the NCC, particularly in the eastern Barents Sea (Loeng et al., 1991).

Sea ice generally covers the area north of the Arctic fronts from late autumn to early summer, with minima and maxima in August/September and March/April, respectively (Loeng, 1991; Smedsrud et al., 2013). The relatively fresh cap created by summer melt stratifies the water column and forms sea ice as it cools to the freezing point during winter. The inflow of Atlantic Water and its associated heat are important in governing sea ice formation (Loeng, 1991; Renner et al., 2018), as are atmospheric factors including northerly winds, cyclone tracks, and air temperatures (Smedsrud et al., 2013, and references therein). Most sea ice in the Barents Sea is formed locally, but some can also be advected from the Arctic Ocean, mainly by wind action (Kwok, 2009). Although strong seasonal and interannual variabilities exist (Vinje, 2001; Divine and Dick, 2006; Smedsrud et al., 2013), the Barents Sea has followed the overall circumpolar trend of recent decreases in sea ice, particularly in the north. Collectively with the Kara Sea, the observed loss has been calculated as $-12.2 \pm 2.1 \times 10^3$ km^2 yr^{-1} over the period 1979–2010 (Cavalieri and Parkinson, 2012).

3. Materials and methods

3.1. Sample selection

This study uses previously published ^{14}C dates on pre-bomb live-collected materials available from the Barents Sea and adjacent regions (Table 1, Table 2). For molluscs, 16 ^{14}C dates (Table 1) were selected from previous publications (Mangerud and Gulliksen, 1975; Foreman and Polyak, 1997; Mangerud et al., 2006) and used for ΔR calculations. Notably, existing ^{14}C dates on deposit-feeding protobranch molluscan genera (e.g., *Portlandia*, *Yoldia*, *Yoldiella*) were excluded from the dataset, as they are prone to enhanced age effects due to their uptake of 'old' detrital carbon, with no systematic offset apparent (Foreman and Polyak, 1997; Dyke et al., 2002, 2003; England et al., 2013). We also excluded omnivores (e.g., *Ischnochiton albae*) and species whose feeding habits are potentially carnivorous (e.g., the gastropod *Solariella obscura*) (Langer, 1978). Ecological information for the molluscan taxa used in our study is given in Table 3. Most selected species are filter feeders, apart from 3 samples which consist of herbivorous grazers (*Margarites groenlandicus*, *Margarites costalis*). Whilst a grazing feeding mode is potentially problematic regarding the ingestion of carbonate material (cf. McConnaughey and Gillikin, 2008), we have retained these samples in our dataset, given the overall sparsity of samples across the region and considering that their available δ^{13}C values fall within the range of marine carbonate (i.e., −1–2‰, extended range −4 to 4‰; Stuiver and Polach, 1977). Following previous approaches to ΔR determination (Mangerud et al., 2006; Coulthard et al., 2010), we assume that molluscs fix their carbon on average 5 years prior to collection; that is, a mollusc live-collected in 1905 is assumed to have (on average) fixed its carbon in 1900. This approach is justified given the known life span of many Arctic molluscs (10–20 years), and *in lieu* of data on the actual age of an individual prior to ^{14}C dating (e.g., by growth band counting; Scourse et al., 2006).

For cetaceans, 19 ^{14}C dates on 18 individuals from Mangerud et al. (2006) were used for ΔR determination (Table 2). Because whales differ in diet and migratory behaviour, with implications for δ^{13}C fractionation and ΔR (Furze et al., 2014), we separated baleen (mysticetes) and toothed (odontocetes) species. Mysticetes have long keratin fringes (baleen) which enable them to ingest large quantities of plankton and small fish by filter feeding (Table 4) (Bannister, 2018; Hooker, 2018). Conversely, odontocetes eat larger prey such as fish, squid and crustaceans, as well as other marine mammals and birds (Table 4) (Kovacs

Table 1
Details of samples used in molluscan ΔR calculations for the Barents Sea. All radiocarbon dates are assumed to have been reported normalized to the terrestrial standard of $\delta^{13}C = -25‰$. Laboratory abbreviations: AA = NSF, Arizona, USA; GX = Geochron Laboratories, USA; T = Trondheim, Norway.

Sample no.	Lab no.	Species	Museum collection designation	Locality	Lat. N (°)	Long. E (°)	Collection depth (m)	Collection year	^{14}C age ± 1σ (^{14}C yrs BP)	$\delta^{13}C$ (‰) VPDB	Comments	Reference
Western Svalbard												
1	T-1537	*Chlamys islandica*	-	Near Bjørnøya	74.1167	19.0667	90	1900	521 ± 34	−0.5		Mangerud and Gulliksen (1975); Mangerud et al. (2006)
2	T-1538	*Chlamys islandica*	-	Bellsund	77.6667	15.0000	120–190	1926	539 ± 37	0.8	Coordinates approximate (c. 77°40′N, 14–16°E)	Mangerud and Gulliksen (1975); Mangerud et al. (2006)
3	T-1539	*Chlamys islandica*	-	Isfjorden	78.1167	14.1333	150–165	1925	517 ± 37	0.5		Mangerud and Gulliksen (1975); Mangerud et al. (2006)
4	T-1540	*Astarte borealis*	-	Adventbukta	78.2500	15.6000	<20	1878	612 ± 50	−0.1		Mangerud and Gulliksen (1975); Mangerud et al. (2006)
5	T-1541	*Astarte borealis*	-	Magdalenafjorden	79.5667	10.6667	40–80	1878	625 ± 45	−0.1		Mangerud and Gulliksen (1975); Mangerud et al. (2006)
Franz Josef Land												
6	GX-19024	*Bathyarca glacialis*	St. Petersburg Zoological 422	N of Salisbury Island	81.2333	53.8500	50	1936	320 ± 50	2.1		Foreman and Polyak (1997)
7	GX-19026	*Margarites groenlandicus*	St. Petersburg Zoological 43	Northbrook Island	79.9167	49.8000	43	1901	347 ± 48	2.4		Foreman and Polyak (1997)
Novaya Zemlya												
8	AA-16839[a]	*Ciliatocardium ciliatum*	St. Petersburg Zoological 91	Krestovaia Bay	74.1667	55.3333	72	1921	550 ± 45	0.0	$\delta^{13}C$ not measured	Foreman and Polyak (1997)
9	GX-19025	*Ciliatocardium ciliatum*	St. Petersburg Zoological 61	Cape Uzkij	73.2000	55.0000	17–35	1926	374 ± 50	0.0		Foreman and Polyak (1997)
10	GX-19208	*Chlamys islandica*	Smithsonian Institution 499,947	Matiushikh Bay	73.2500	53.3333	not given	1937	453 ± 58	1.0		Foreman and Polyak (1997)
11	AA-16843[a]	*Margarites groenlandicus*	St. Petersburg Zoological 205	Mal Karmakuly	72.3667	52.7500	9–18	1900	400 ± 50	0.0	$\delta^{13}C$ not measured	Foreman and Polyak (1997)
12	GX-19206	*Margarites costalis*	St. Petersburg Zoological 106	Belushia Bay	71.5000	52.4167	13–15	1923	474 ± 59	2.0	Erroneously reported as "*Marginatus costalis*"	Foreman and Polyak (1997)
NorthernNorway												
13	T-1536	*Astarte crenata*	-	Vadsø	70.0667	29.7500	<10	1857	541 ± 36	−0.5		Mangerud and Gulliksen (1975); Mangerud et al. (2006)
14	T-1535	*Astarte crenata*	-	Tanafjord	70.5000	28.6667	232	1876	576 ± 47	1.1	Coordinates approximate (c. 70°30′N, c. 28°40′E)	Mangerud and Gulliksen (1975); Mangerud et al. (2006)
15	T-958	*Mytilus edulis*	-	Komagfjord	70.2667	23.4000	0–10	1922	546 ± 57	0.0		Mangerud and Gulliksen (1975); Mangerud et al. (2006)
16	T-1534	*Chlamys islandica*	-	Tromsø	69.6500	18.3000	<10	1857	548 ± 37	0.2		Mangerud and Gulliksen (1975); Mangerud et al. (2006)

[a] $\delta^{13}C$ not measured but assumed as 0‰.

et al., 2004; Hooker, 2018). Ecological information for individual species used in this study is provided in Table 4. Ideally, different ΔR values should be calculated for individual species, given differing seasonal feeding strategies and migration ranges and the consequent incorporation of carbon from water masses of different ages (Furze et al., 2014). However, the limited number of samples in this dataset (Table 2) precludes this approach. As a first approximation, we calculate ΔR for grouped baleen and toothed whales, as well as providing a combined ΔR for all cetaceans in the dataset. Samples selected from Mangerud et al. (2006) for ΔR calculation were collected between 48°N and 71°N, and 5°W and 31°E (Fig. 2) and are considered representative given the broad migration area of those species (Table 4). Most of the species used in this study seasonally migrate between the mid- and high-latitude North Atlantic Ocean (Storrie et al., 2018; Whitehead, 2018), e.g., from the Mediterranean Sea and the Gulf of Mexico to Jan Mayen and Svalbard for fin whales (*Balaenoptera physalus*; Storrie et al., 2018; Kovacs et al., 2004). Sperm (*Physeter macrocephalus*) and killer (*Orcinus orca*) whales have an uncertain, but broader migration area compared to other species in this study. They have been observed seasonally around Svalbard (Storrie et al., 2018), but both are also found in lower latitudes. Female sperm whales have been observed south of 40°N, whereas killer whales occur around high-productivity coastlines globally (Kovacs et al., 2004; Bannister et al., 2018).

Two whale dates from Mangerud et al. (2006) were excluded (T-13246, *Mesoplodon bidens*; T-13226, *Eubalaena glacialis*) due to the absence of these species in Svalbard-Barents Sea waters (Kovacs et al., 2004; Kenney, 2009; Storrie et al., 2018). A further date (T-13236, juvenile *Balaenoptera acutorostrata*) was rejected due to potential enhanced inter-seasonal $\delta^{13}C$ variations characteristic of juvenile baleen whales, as demonstrated in bowheads (*Balaena mysticetus*; Schell et al., 1989). Two dates in Mangerud et al. (2006) on *Balaenoptera musculus* (T-13230, T-13231) were from the same individual. For the sake of this study, these two dates (Table 2) were averaged, and their errors combined prior to ΔR calculation. For calibration purposes, we assume that all adult cetaceans fixed their carbon 10 years before death (i.e., a decade before collection date), following Mangerud et al. (2006).

3.2. Calculations

Molluscan-based ΔR values are primarily defined by regional oceanography (Alves et al., 2018), with the common approach being to divide an area into specific oceanographic sectors for which regional ΔR (ΔR_R) values are calculated based on local ΔR (ΔR_L) data points (e.g., Coulthard et al., 2010). However, the scarcity of available molluscan data points (Fig. 1) in some parts of our study area (e.g., eastern Svalbard, central Barents Sea) can result in oceanographically defined regions for which no meaningful ΔR_R can be calculated. Recommendations on how to treat these areas are given in the Discussion. We have identified four broad sectors with differing oceanographic influences: 1) western Svalbard including Bjørnøya, north of the BSAF and heavily influenced by Atlantic water from the WSC (n = 5); 2) Franz Josef Land situated north of the BSAF and receiving Arctic Ocean water (n = 2); 3) Novaya Zemlya also north of the BSAF, yet influenced by both polar and Atlantic water (n = 5); and 4) northern Norway which is south of the BSAF, characterized by the NCaC and Atlantic water modified from runoff from land (n = 4; Fig. 1).

For molluscs, individual ΔR_L were determined by Equation (1), using both Marine20 (Heaton et al., 2020) and Marine13 (Reimer et al., 2013) calibration curves. As these curves only provide ^{14}C ages in 10 and 5 calendar year steps, respectively, age values and their associated standard deviations falling between these points were interpolated linearly. The standard deviation of ΔR_L, σ_L, is calculated by Equation (2) using the Gaussian law of error propagation. For both equations (1) and (2), 'cal curve' refers to the marine calibration curve and the appropriate age (^{14}C) and standard deviation (σ) at the equivalent calendar year.

$$\Delta R_L = {}^{14}C_{sample} - {}^{14}C_{cal\ curve} \quad (1)$$

(after Stuiver et al., 1986).

$$\sigma_L = \sqrt{\sigma^2_{sample} + \sigma^2_{cal\ curve}} \quad (2)$$

(after Bevington and Robinson, 2002).

Error-weighted pooled mean ΔR_R values were subsequently calculated from individual ΔR_L for each of the four areas using Equation (3) for Marine20 (Heaton et al., 2020) and Marine13 (Reimer et al., 2013) calibration curves. The standard deviation of the ΔR_R values was determined by the larger value of either the pooled standard deviation of the mean (Equation (4)) or the square root of the weighted average variance (Equation (5)). The internal variability of the data was assessed by calculating X^2 (Equation (6); after Ward and Wilson, 1978). Following Bondevik and Gulliksen in Mangerud et al. (2006) and Coulthard et al. (2010), X^2 is given according to critical acceptance values and normalized by dividing it by the number of degrees of freedom (n − 1) in the respective dataset for each region. If $X^2/(n-1) \leq 1$, uncertainties in the measurements within the dataset explain the variability. Additional variability (beyond measurement uncertainties) exist if $X^2/(n-1) \geq 1$.

$$\Delta R_R = \frac{\sum_{i=1}^{n} \Delta R_{L_i} / \sigma^2_{L_i}}{\sum_{i=1}^{n} 1 / \sigma^2_{L_i}} \quad (3)$$

(after Bevington and Robinson, 2002).

$$S_{pooled} = \sqrt{\frac{1}{\sum_{i=1}^{n} 1 / \sigma^2_{L_i}}} \quad (4)$$

(after Bevington and Robinson, 2002).

$$\sigma_R = \sqrt{\frac{n}{n-1} \frac{\sum_{i=1}^{n} \left(\frac{\Delta R_{L_i} - \Delta R_R}{\sigma_{L_i}}\right)^2}{\sum_{i=1}^{n} 1 / \sigma^2_{L_i}}} \quad (5)$$

(after Bevington and Robinson, 2002).

$$X^2 = \sum_{i=1}^{n} \frac{(\Delta R_{L_i} - \Delta R_R)^2}{{\sigma_{L_i}}^2} \quad (6)$$

(after Bondevik and Gulliksen in Mangerud et al., 2006).

For Equations (3)–(6), σ_L is the standard deviation for ΔR_L, s_{pooled} is the standard deviation of the mean, and σ_R is the square root of the weighted average variance. The larger of s_{pooled} or σ_R is considered the standard deviation of ΔR_R.

Methodology for cetaceans followed that of molluscs (equations (1)–(6)), with whales divided into two populations – toothed and baleen ($n_{toothed} = 10$; $n_{baleen} = 8$). ΔR_R and associated standard deviation were calculated for both populations as well as for all combined whales (n = 18). Unlike sessile molluscs, no regional oceanographic subdivisions were defined or calculated for whales, given the extensive and broad geographical ranges of these mobile marine mammals.

4. Results

Regional ΔR values and their details are given in Tables 5 and 6, whereas a summary of recommended values is provided in Table 7. For Marine20 (Heaton et al., 2020), regional molluscan ΔR values vary between −277 ± 57 and −61 ± 37 ^{14}C yrs; for Marine13 (Reimer et al., 2013), they range from −122 ± 38 to 94 ± 38 ^{14}C yrs. For both calibration curves, most negative values occur on Franz Josef Land, whereas highest ΔR_R are found on western Svalbard, an area dominated by Atlantic Water from the northward-flowing SB current. In contrast,

Table 2
Sample details of whale-based dates used in cetacean ΔR calculations for the Barents Sea. All radiocarbon dates are assumed to have been reported normalized to the terrestrial standard of $\delta^{13}C = -25‰$. Laboratory abbreviation: T = Trondheim, Norway. All data are from Mangerud et al. (2006).

Sample no.	Lab no.	Species	Common name	Bergen Museum sample no.	Locality	Lat. N (°)	Long. E (°)	Collection year	Dated part	^{14}C age ± 1σ (^{14}C yrs BP)	$\delta^{13}C$ (‰) VPDB
Odontoceti (toothed whales)											
1	T-13228	*Physeter macrocephalus*	Sperm whale	59	Bretagne	48.0000	5.0000	1890	Skull	438 ± 23	−12.4
2	T-13241	*Hyperoodon ampullatus*	Northern bottlenose whale	871	Oslo	59.8833	10.6667	1874	Skull	543 ± 24	−18.3
3	T-13242	*Globicephala melas*	Pilot whale	879	Møgster	60.0667	5.0833	1874	Skull	503 ± 32	−12.2
4	T-13227	*Globicephala melas*	Pilot whale	33	Bildøy	60.3500	5.2333	1893	Vertebra 1	466 ± 23	−13.0
5	T-13237	*Lagenorhynchus albirostris*	White-beaked dolphin	680	Bildøy	60.3500	5.2333	1887	Humerus	486 ± 24	−16.5
6	T-13243	*Orcinus orca*	Killer whale	889	Bildøy	60.3500	5.2333	1860	Skull	478 ± 29	−13.0
7	T-13235	*Orcinus orca*	Killer whale	564	Bildøy	60.3500	5.2333	1887	Rib	477 ± 22	−17.3
8	T-13238	*Lagenorhynchus acutus*	Atlantic white-sided dolphin	722	Toska	60.6000	4.9333	1885	Vertebra 1	491 ± 53	−15.5
9	T-13229	*Hyperoodon ampullatus*	Northern bottlenose whale	419	Kilstraumen	60.8167	4.9500	1884	Skull	505 ± 21	−14.7
10	T-13245	*Physeter macrocephalus*	Sperm whale	1393	Båtsfjord	70.6333	29.8333	1896	Rib	376 ± 28	−13.3
Mysticeti (baleen whales)											
11	T-13234	*Balaenoptera physalus*	Fin whale	423	Utsira	59.3167	4.8833	1865	Mandible	533 ± 22	−13.5
12	T-13240	*Balaenoptera acutorostrata*	Minke whale	870	Skogsvåg	60.2667	5.0833	1869	Skull	420 ± 31	−15.3
13	T-13239	*Balaenoptera acutorostrata*	Minke whale	869	Skogsvåg	60.2667	5.0833	1860	Skull	441 ± 32	−14.4
14	T-13233	*Balaenoptera physalus*	Fin whale	424	Florø	61.5833	5.0167	1867	Mandible	523 ± 24	−14.8
15	T-13232	*Balaenoptera borealis*	Sei whale	421	Sørøya	70.6333	22.0000	1879	Mandible	479 ± 20	−16.6
16	T-13244	*Balaenoptera borealis*	Sei whale	983	Sørvær	70.6333	22.0000	1894	Ear bone	527 ± 50	−16.1
17	T-13230[a]	*Balaenoptera musculus*	Blue whale	420	Finnmark	71.0000	27.0000	1879	Mandible	470 ± 23	−15.9
18	T-13231[a]	*Balaenoptera musculus*	Blue whale	420	Finnmark	71.0000	27.0000	1879	Vertebr 49	489 ± 21	−17.7
19	T-13247	*Megaptera novaeangliae*	Humpback whale	3821	Vardø	70.3833	31.0833	1883	Mandible	489 ± 32	−15.5

[a] These dates are from the same individual.

Table 3
Ecology of molluscs species used in ΔR calculations.

Species	Common name	Age span (yrs)	Feeding ecology	Habit	Substrate	References
Astarte borealis (Schumacher, 1817)	boreal astarte	8–10	suspension	infaunal	sand, muddy gravel, sandy gravel	Peacock (1993); Selin (2007)
Astarte crenata (Gray, 1824)	crenulate astarte		suspension	infaunal	sand, muddy gravel, sandy gravel	Peacock (1993)
Bathyarca glacialis (Gray, 1824)	glacial bathyark		suspension	epifaunal		Peacock (1993)
Chlamys islandica (O. F. Müller, 1776)	Iceland scallop	18–23	suspension	epifaunal		Peacock (1993); Shumway and Parsons (2006)
Ciliatocardium ciliatum (Fabricius, 1780)	hairy cockle		suspension	infaunal		Peacock (1993)
Margarites costalis (Gould, 1841)			grazing (seaweed detritus)			Smith et al. (1985)
Margarites groenlandicus (Gmelin, 1791)			grazing (bacteria)			Paar et al. (2019)
Mytilus edulis Linnaeus, 1758	blue mussel, edible mussel	max. 13	suspension	epifaunal	rock	Peacock (1993); Zotin and Ozernyuk (2004)

Franz Josef Land, the most northerly locale in our Barents Sea dataset and displaying the lowest ΔR_R values, is influenced by Arctic Water via both the Arctic Ocean and the NBSO, though some Atlantic-source water from the eastward-continuing SB also reaches the northern part of this archipelago. Values for Novaya Zemlya and northern Norway are closer to those from western Svalbard and overlap at 1σ (Table 5). Notable are the consistently negative molluscan ΔR_R values derived from the Marine20 calibration curve, a result of the high global R values in Marine20 (Heaton et al., 2020) compared to Marine13 (Reimer et al., 2013), an aspect elaborated on in the Discussion. Uncertainties in the measurements within the dataset explain the variability for all four regions (i.e., $X^2/(n-1) \leq 1$, Table 5). The only exception to this is Novaya Zemlya when calculated using Marine13 which shows $X^2/(n-1) > 1$ (1.78).

ΔR_R values for both baleen and toothed whales are very similar, with 8 ± 41 ^{14}C yrs and 1 ± 41 ^{14}C yrs respectively for Marine13 (Reimer et al., 2013); for Marine20 (Heaton et al., 2020) they are -158 ± 43 ^{14}C yrs and -161 ± 41 ^{14}C yrs, respectively. Combined (toothed + baleen) ΔR_R values are 4 ± 49 ^{14}C yrs for Marine13 and -160 ± 41 ^{14}C yrs for Marine20. Measurement uncertainties within the dataset can explain the variability (i.e., $X^2/(n-1) \leq 1$) for all populations (including combined) for Marine20 (Table 6). However, the reverse is true for Marine13, as all $X^2/(n-1)$ values are >1 (Table 6).

5. Discussion

5.1. Revised molluscan ΔR values for the Barents Sea

Our new ΔR values provide an overdue assessment of regional Late Holocene marine-terrestrial ^{14}C offsets in a region at the centre of recent and ongoing climate change and relevant to global climate (e.g., Smedsrud et al., 2013; Comiso and Hall, 2014). We calculated mollusc-based ΔR_R for the two most recent iterations of the marine calibration curve, Marine 13 (Reimer et al., 2013) and Marine20 (Heaton et al., 2020). The recommended values (Table 7) are as follows: western Svalbard (including Bjørnøya), -61 ± 37 ^{14}C yrs (Marine20) and 94 ± 38 ^{14}C yrs (Marine13); Franz Josef Land, -277 ± 57 ^{14}C yrs (Marine20) and -122 ± 38 ^{14}C yrs (Marine13); Novaya Zemlya, -156 ± 73 ^{14}C yrs (Marine20) and 0 ± 76 ^{14}C yrs (Marine13); northern Norway, -86 ± 39 ^{14}C yrs (Marine20) and 74 ± 24 ^{14}C yrs (Marine13).

The number of samples in each dataset and the geographic distribution of data points highlight existing gaps in data coverage, as well as clustering in some areas (Fig. 1). For example, the dataset from western Svalbard comprises five samples, two of which are from the same fjord (samples 3 and 4, Fig. 1, Table 1). Conversely, no samples are currently available from either the northern or eastern coasts of the Svalbard archipelago, or from the central Barents Sea. While both the clustering and the data sparsity may potentially hinder more specific ΔR_R calculation for these areas, the four molluscan-based datasets nevertheless broadly represent the oceanographic influence prevalent in their settings (Ingvaldsen and Loeng, 2009; Smedsrud et al., 2013): western Svalbard with its strong Atlantic water influence; Franz Josef Land receiving Arctic Ocean water; Novaya Zemlya influenced by both Atlantic and polar water and situated north of the BSAF; and the northern Norway coast impacted by the NCaC. Therefore, *in lieu* of additional datapoints from dated pre-bomb live-collected molluscs, our newly calculated ΔR_R values should be considered the best available approximation.

Of the four regions for which molluscan ΔR_R terms were calculated, the Novaya Zemlya archipelago is the only one whose variability was not captured by existing samples (i.e., $X^2/(n-1) > 1$) for the Marine13 calibration curve. However, this was not the case for Marine20, suggesting that the modelling approach used by Heaton et al. (2020) to generate the calibration curve better captures the time-variant nature of R in comparison to the earlier version (Reimer et al., 2013). Undoubtedly, more ΔR_L datapoints from along the Novaya Zemlya coast would improve the accuracy of ΔR_R for this archipelago, additionally also reducing the size of the current error. Furthermore, a more

Table 4
Ecology of whale species used in ΔR calculations.

Species	Common name	Age span (yrs)	Feeding ecology	Migration routes	References
Odontoceti (toothed whales)					
Globicephala melas (Traill, 1809)	Pilot whale	♀ 60 ♂ 35-45	Squid, Atlantic cod, Greenland turbot, Greenland halibut, Atlantic mackerel, Atlantic herring, hake, silver hake, Atlantic Argentine, blue whiting	Greenland-Iceland-Barents Sea region-south of Svalbard	Kovacs et al. (2004); Olson (2018)
Hyperoodon ampullatus (Forster, 1770)	Northern bottlenose whale	unknown	Squid, sea cucumbers, fish, shrimp	UK-France-northeast Atlantic-offshore western Svalbard	Kovacs et al. (2004)
Lagenorhynchus acutus (Gray, 1828)	Atlantic white-sided dolphin	♀ ≤ 27 ♂ ≤ 22	Herring, small mackerel, gadid fish, smelts, hake, sand lances, squid	western British Iles-northern Europe-Norwegian Sea-Svalbard	Cipriano (2018); Storrie et al. (2018)
Lagenorhynchus albirostris (Gray, 1846)	White-beaked dolphin	♀ <34	Gadid fish, cephaloopods, benthic crustaceans	Massachusetts-Greenland-Iceland-British Isles-south Denmark-southern and western Svalbard	Kovacs et al. (2004); Kinze (2018)
Orcinus orca (Linnaeus, 1758)	Killer whale	♀ 50 (max. 80–90) ♂ 29 (max. 50–60)	Marine mammals, salmon, herring, cod, tuna, sharks, squid, octopus, sea turtles, sea birds	Northwestern American coast-Aleutian Islands-northern Norway-Spitsbergen fjords and offshore	Kovacs (2004); Ford (2018)
Physeter macrocephalus Linnaeus, 1758	Sperm whale	ca. >50, 70 (?)	Squid (♀: giant and jumbo; ♂: colossal), histiotheutid squid, demersal (♂: sharks, rays, gadoids) and mesopelagic fish	♀: below 40°N ♂: south of sea-ice limit in North Atlantic and Svalbard	Kovacs et al. (2004); Storrie et al. (2018); Whitehead (2018)
Mysticeti (baleen whales)					
Balaenoptera acutorostrata Lacépède, 1804	Minke whale	unknown	Sand lances, sand eel, capelin, mackerel, cod, coal fish, whiting, sprat, wolffish, dogfish, pollack, haddock, herring, euphausiids, copepods	Strait of Gibraltar-Svalbard	Kovacs (2004); Perrin et al. (2018)
Balaenoptera borealis Lesson, 1828	Sei whale	unknown	Euphausiids, copepods, fish, squid	UK and Norwegian coasts-Iceland-Greenland-Iceland-Greenland-Svalbard	Horwood (2018); Storrie et al. (2018)
Balaenoptera musculus (Linnaeus, 1758)	Blue whale	80–90	Krill	Azores-Iceland-Jan Mayen-Spitsbergen	Kovacs (2004); Sears and Perrin (2018)
Balaenoptera physalus (Linnaeus, 1758)	Fin whale	80–100	Krill and other planktonic crustaceans, capelin, herring, mackerel, blue whiting, small squid	Gulf of Mexico-Mediterranean-Spain-Portugal-British Isles-east Greenland-Iceland-Faroe Islands-Jan Mayen-Svalbard	Kovacs (2004); Aguilar and García-Vernet (2018); Storrie et al. (2018)
Megaptera novaeangliae (Borowski, 1781)	Humpback whale	50	Euphausiids, herring, capelin, sand lances, mackerel	Tropics-Gulf of Maine-Svalbard	Kovacs et al. (2004); Clapham (2018)

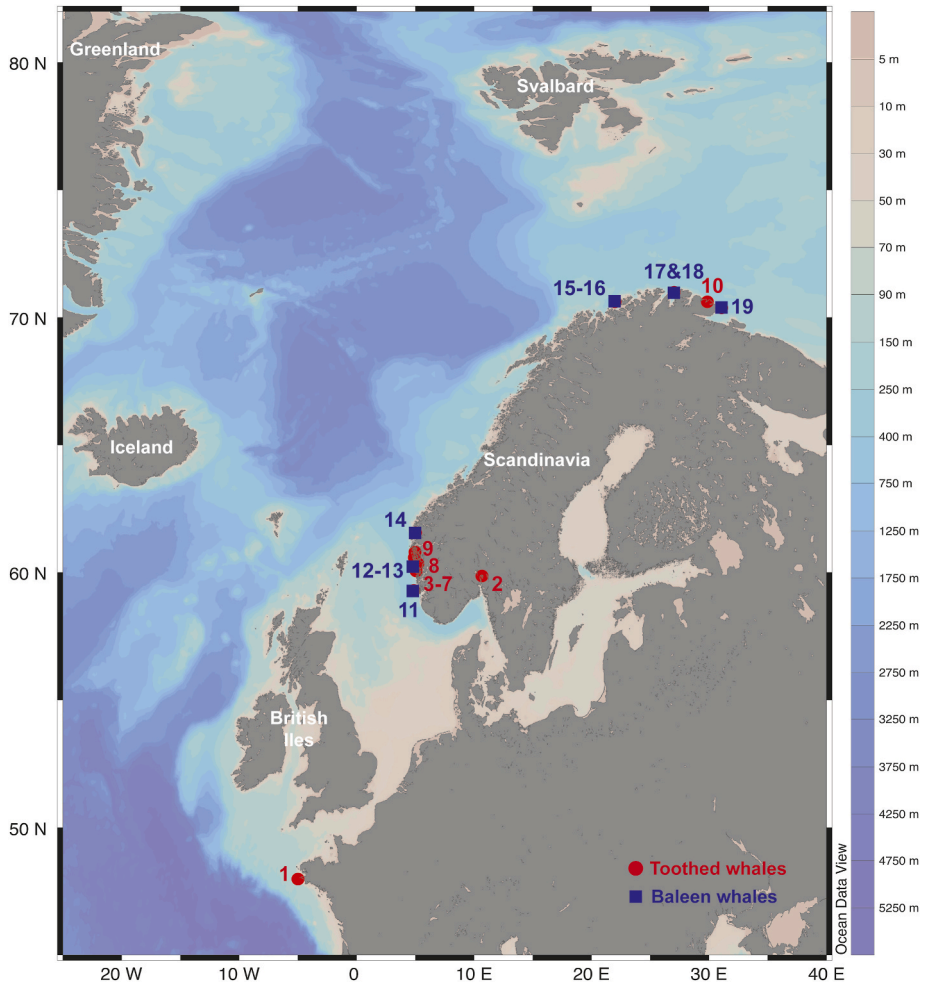

Fig. 2. Map of the northern North Atlantic, showing sites of available pre-bomb collected and radiocarbon dated cetacean samples. Toothed and baleen whales are denoted by red circles and blue squares, respectively. Site numbers correspond to those in Table 2. The base map was drawn in Ocean Data View (Schlitzer, 2020).

comprehensive dataset from across the Barents Sea is desirable, especially for areas that currently have very few ΔR_L datapoints (e.g., Franz Josef Land), or none at all (e.g., central Barents Sea and eastern Svalbard). It must be emphasized that improving the accuracy and precision of ΔR_R beyond that calculated here requires a major expansion of the database of ^{14}C-dated live-collected marine carbonate materials into areas that hitherto have few or no datapoints. This would necessitate a dedicated project focused on identifying and accessing collections from historic, pre-1956 scientific expeditions and other live-collecting initiatives, with permission to perform destructive analyses, even if recent advances in AMS ^{14}C dating have significantly reduced the amount of material needed for accurate and precise radiocarbon dates (Wood, 2015). In the meantime, our calculated values provide a long overdue revision of molluscan ΔR_R for the Barents Sea region.

5.2. *Whale-based ΔR values*

Our calculated ΔR for cetaceans provide revised calibration terms for Barents Sea baleen and toothed whales, with the potential to further improve and constrain regional sea-level curves and deglacial timing across the area (e.g., Forman, 1990; Forman et al., 2004; Farnsworth et al., 2020), as well as informing archaeological studies (e.g., Jørgensen, 2005; Haquebord and Avango, 2016). The recommended values (Table 7) are: mysticetes, −158 ± 43 ^{14}C yrs (Marine20), 8 ± 41 ^{14}C yrs (Marine13); odontocetes, −161 ± 41 ^{14}C yrs (Marine20), 1 ± 41 ^{14}C yrs (Marine13); combined baleen and toothed whales, −160 ± 41 ^{14}C yrs (Marine20), 4 ± 49 ^{14}C yrs (Marine13).

All cetacean species used in our calculations regularly occur around Svalbard and the Barents Sea (Kovacs et al., 2004), even if only four of the 18 individuals were caught along the Barents Sea coast (northern Norway) and none were collected directly from Svalbard, Franz Josef Land, or Novaya Zemlya (Fig. 2). Furthermore, despite our values being derived from species with differing migratory ranges and diets (even within feeding mode groups), the similarity between toothed and baleen whale ΔR suggests that these differences contribute minimally to variability in cetacean reservoir age. The internal variability of the existing whale data ($X^2/(n-1)$) is explained by the measurement uncertainties within the Marine20-based datasets (Table 6). However, while being close to 1, $X^2/(n-1)$ for all three calculated Marine13-based cetacean ΔR_R terms indicates that additional variability beyond measurement uncertainties exists. Similar to our molluscan analyses, this implies that Marine20 (Heaton et al., 2020) better approximates temporal variations in R than does Marine13 (Reimer et al., 2013), despite the later calibration curve only reporting annually-defined ^{14}C ages for the latest Holocene every 10 calendar years as opposed to every 5 years for Marine13.

We recognize that the cetacean dataset is limited spatially and numerically. More datapoints are required to further refine appropriate ΔR terms for whales. Ideally, such determinations should be species-specific, and thus would incorporate both autecological factors and vital effects into a taxon-appropriate ΔR, an approach successfully demonstrated in other regions (Furze et al., 2014). The bowhead or Greenland right whale, *Balaena mysticetus*, that was the mainstay of the historic Svalbard whaling industry and occurs frequently in 17th to 19th

Table 5
Results of molluscan ΔR calculations.

Sample no.	Sample designation	Species	^{14}C age ± error (^{14}C yrs BP)	Year of collection/ death (yr CE)	Year of C fixing (yr CE)	MARINE13								MARINE20							
						Marine reservoir age ± error (^{14}C yrs) @ yr of C fixing	ΔR_L (^{14}C yrs)	ΔR_L 1σ (^{14}C yrs)	ΔR_R (^{14}C yrs)	s_{pooled} (^{14}C yrs)	σ_R (^{14}C yrs)	X^2	X^2/(n-1)	Marine reservoir age ± error (^{14}C yrs) @ yr of C fixing	ΔR_L (^{14}C yrs)	ΔR_L 1σ (^{14}C yrs)	ΔR_R (^{14}C yrs)	s_{pooled} (^{14}C yrs)	σ_R (^{14}C yrs)	X^2	X^2/(n-1)
Western Svalbard																					
1	T-1537	*Chlamys islandica*	521 ± 34	1900	1895	460 ± 23	61.00	41.05	94.25	20.55	37.99	2.73	0.68	618.71 ± 64.37	−97.71	72.80	−60.61	33.88	36.84	0.95	0.24
2	T-1538	*Chlamys islandica*	539 ± 37	1926	1921	448.6 ± 23	90.40	43.57						604.31 ± 63.72	−65.31	73.68					
3	T-1539	*Chlamys islandica*	517 ± 37	1925	1920	448 ± 23	69.00	43.57						604.33 ± 62.88	−87.33	72.96					
4	T-1540	*Astarte borealis*	612 ± 50	1878	1873	476.2 ± 23	135.80	55.04						637.83 ± 64.74	−25.83	81.80					
5	T-1541	*Astarte borealis*	625 ± 45	1878	1873	476.2 ± 23	148.80	50.54						637.83 ± 64.74	−12.83	78.84					
Franz Josef Land																					
6	GX-19024	*Bathyarca glacialis*	320 ± 50	1936	1931	453.8 ± 23	−133.80	55.04	−122.43	38.26	15.55	0.08	0.08	603.95 ± 62.77	−283.95	80.25	−277.31	56.76	9.40	0.01	0.01
7	GX-19026	*Margarites groenlandicus*	347 ± 48	1901	1896	458.8 ± 23	−111.80	53.23						617.66 ± 64.36	−270.66	80.29					
Novaya Zemlya																					
8	AA-16839	*Ciliatocardium ciliatum*	550 ± 46	1921	1916	448 ± 23	102.00	51.43	0.13	25.44	75.95	7.13	1.78	605.36 ± 63.25	−55.36	78.21	−156.31	36.82	73.38	3.18	0.79
9	GX-19025	*Ciliatocardium ciliatum*	374 ± 50	1926	1921	448.6 ± 23	−74.60	55.04						604.31 ± 63.72	−230.31	81.00					
10	GX-19208	*Chlamys islandica*	453 ± 58	1937	1932	454.6 ± 23	−1.60	62.39						603.79 ± 62.65	−150.79	85.38					
11	AA-16843	*Margarites groenlandicus*	400 ± 50	1900	1895	460 ± 23	−60.00	55.04						618.71 ± 64.37	−218.71	81.51					
12	GX-19206	*Margarites costalis*	474 ± 59	1923	1918	448 ± 23	26.00	63.32						604.85 ± 63.07	−130.85	86.36					
NorthernNorway																					
13	T-1536	*Astarte crenata*	541 ± 36	1857	1852	484.2 ± 23	56.80	42.72	74.32	24.22	21.49	0.59	0.20	651.49 ± 65.48	−110.49	74.72	−86.34	39.22	26.47	0.34	0.11
14	T-1535	*Astarte crenata*	576 ± 47	1876	1871	477.4 ± 23	98.60	52.33						639.31 ± 64.79	−63.31	80.04					
15	T-958	*Mytilus edulis*	546 ± 57	1922	1917	448 ± 23	98.00	61.47						605.1 ± 63.16	−59.10	85.08					
16	T-1534	*Chlamys islandica*	548 ± 37	1857	1852	484.2 ± 23	63.80	43.57						651.49 ± 65.48	−103.49	75.21					

Table 6
Results of whale-based ΔR_L and ΔR_R calculations.

Sample no.	Sample designation	Species	^{14}C age ± error (^{14}C yrs BP)	Year of collection/ death (yr CE)	Year of C fixing (yr CE)	MARINE13							MARINE20						
						Marine reservoir age ± error (^{14}C yrs) @ yr of C fixing	ΔR_L (^{14}C yrs)	ΔR_L 1σ (^{14}C yrs)	ΔR_R (^{14}C yrs)	s_{pooled} (^{14}C yrs)	σ_R (^{14}C yrs)	X^2	X^2/ (n-1)	Marine reservoir age ± error (^{14}C yrs) @ yr of C fixing	ΔR_L (^{14}C yrs)	ΔR_L 1σ (^{14}C yrs)	ΔR_R (^{14}C yrs)	s_{pooled} (14C yrs)	σ_R (^{14}C yrs)	X^2	X^2/ (n-1)
Odontoceti (toothed whales)																			
1	T-13228	*Physeter macrocephalus*	438 ± 23	1890	1880	473 ± 23	−35	32.53					632.65 ± 64.56	−194.65	68.53				
2	T-13241	*Hyperoodon ampullatus*	543 ± 24	1874	1864	480.2 ± 23	62.80	33.24					643.88 ± 65.02	−100.88	69.31				
3	T-13242	*Globicephala melas*	503 ± 32	1874	1864	480.2 ± 23	22.80	39.41	1.06	11.09	41.44	12.57	1.40	643.88 ± 65.02	−140.88	72.47	−161.37	22.33	40.86	3.01	0.33
4	T-13227	*Globicephala melas*	466 ± 23	1893	1883	470 ± 23	−4.00	32.53						630.04 ± 64.51	−164.04	68.49					
5	T-13237	*Lagenorhynchus albirostris*	486 ± 24	1887	1877	474.2 ± 23	11.80	33.24						634.87 ± 64.64	−148.87	68.95					
6	T-13243	*Orcinus orca*	478 ± 29	1860	1850	485 ± 24	−7.00	37.64						652.76 ± 65.56	−174.76	71.69					
7	T-13235	*Orcinus orca*	477 ± 22	1887	1877	474.2 ± 23	2.80	31.83						634.87 ± 64.64	−157.87	68.28					
8	T-13238	*Lagenorhynchus acutus*	491 ± 53	1885	1875	475 ± 23	16.00	57.78						636.35 ± 64.69	−145.35	83.63					
9	T-13229	*Hyperoodon ampullatus*	505 ± 21	1884	1874	475.6 ± 23	29.40	31.14						637.09 ± 64.72	−132.09	68.04					
10	T-13245	*Physeter macrocephalus*	376 ± 28	1896	1886	467.4 ± 23	−91.40	36.24						627.43 ± 64.45	−251.43	70.27					
Mysticeti (baleen whales)																			
11	T-13234	*Balaenoptera physalus*	533 ± 22	1865	1855	483 ± 23	50.00	31.83						649.60 ± 65.36	−116.60	68.96					
12	T-13240	*Balaenoptera acutorostrata*	420 ± 31	1869	1859	481.4 ± 23	−61.40	38.60	7.84	13.01	40.71	8.57	1.22	647.06 ± 65.19	−227.06	72.19	−157.46	25.40	43.18	2.53	0.36
13	T-13239	*Balaenoptera acutorostrata*	441 ± 32	1860	1850	485 ± 24	−44.00	40.00						652.76 ± 65.56	−211.76	72.95					
14	T-13233	*Balaenoptera physalus*	523 ± 24	1867	1857	482.2 ± 23	40.80	33.24						648.33 ± 65.27	−125.33	69.54					
15	T-13232	*Balaenoptera borealis*	479 ± 20	1879	1869	478.4 ± 23	0.60	30.48						640.69 ± 64.85	−161.69	67.86					
16	T-13244	*Balaenoptera borealis*	527 ± 50	1894	1884	469 ± 23	58.00	55.04						629.17 ± 64.49	−102.17	81.60					
17 & 18	T-13230 & T-13231 average	*Balaenoptera musculus*	479.5 ± 31	1879	1869	478.4 ± 23	1.10	38.60						640.69 ± 64.85	−161.19	71.88					
19	T-13247	*Megaptera novaeangliae*	489 ± 32	1883	1873	476.2 ± 23	12.80	39.41						637.83 ± 64.74	−148.83	72.22					
Combined (toothed + baleen whales)																			
									3.92	8.44	48.81	21.13	1.17				−159.67	16.77	40.63	5.54	0.62

Table 7
Recommended ΔR values for the Barents Sea for molluscs and whales.

Material	Region/Group	MARINE13					MARINE20				
		ΔR_R (^{14}C yrs)	s_{pooled} (^{14}C yrs)	σ_R (^{14}C yrs)	X^2/(n-1)	Recommended ΔR_R value (^{14}C yrs)	ΔR_R (^{14}C yrs)	s_{pooled} (^{14}C yrs)	σ_R (^{14}C yrs)	X^2/(n-1)	Recommended ΔR_R value (^{14}C yrs)
MOLLUSCS	West Svalbard	94.25	20.55	37.99	0.68	**94 ± 38**	−60.61	33.88	36.84	0.24	**−61 ± 37**
	Franz Josef Land	−122.43	38.26	15.55	0.08	**−122 ± 38**	−277.31	56.76	9.40	0.01	**−277 ± 57**
	Novaya Zemlya	0.13	25.44	75.95	1.78	**0 ± 76**	−156.31	36.82	73.38	0.80	**−156 ± 73**
	North Norway	74.32	24.22	21.49	0.20	**74 ± 24**	−86.34	39.22	26.47	0.11	**−86 ± 39**
CETACEANS	Toothed whales	1.06	11.09	41.44	1.40	**1 ± 41**	−161.38	22.33	40.86	0.34	**−161 ± 41**
	Baleen whales	7.84	13.01	40.71	1.22	**8 ± 41**	−157.47	25.40	43.18	0.36	**−158 ± 43**
	Combined (toothed + baleen)	3.92	8.44	48.81	1.74	**4 ± 49**	−159.67	16.77	40.63	0.62	**−160 ± 41**

century archaeological sites in the archipelago (Hacquebord, 2001; Hacquebord and Avango, 2016), is absent from the dataset. Given its large size and pre-whaling abundance (Hacquebord, 1999), this species also likely constitutes most large whalebone finds on Svalbard's isostatically-emergent shorelines (though rarely identified to species level in the literature) on which deglacial and sea-level chronologies are, to a large extent, based (e.g., Forman, 1990; Forman et al., 2004). Including *B. mysticetus* in this dataset, and ideally deriving a bowhead-specific ΔR, would be extremely valuable, as would be the inclusion of common smaller odontocetes with comparatively limited migratory ranges, such as beluga (*Delphinapterus leucas*; Boltunov and Belikov, 2002). In the absence of such an extended dataset, our cetacean ΔR values provide a useful and up-to-date tool for the calibration of whale-based radiocarbon dates and thus improved archaeological and Quaternary geological chronologies.

5.3. Considerations for using Marine20-derived ΔR values

Marine archives reflect ^{14}C in dissolved organic carbon and not atmospheric ^{14}C directly (e.g., Stuiver et al., 1986). This has been addressed when developing marine radiocarbon calibration curves using models of ocean ^{14}C mixing, combined with tree ring records and other archives with robust independent age control such as speleothems (Hughen et al., 2004; Reimer et al., 2009, 2013). For the latest iteration, Marine20, Heaton et al. (2020) have applied the BICYCLE global carbon cycle model, thereby avoiding splicing different sections of the marine radiocarbon curve together as previously (e.g., Reimer et al., 2013). However, like earlier iterations of the marine calibration curve (Reimer et al., 2009, 2013), the Marine20 model of global average marine reservoir age through time is, *sensu stricto*, restricted to subtropical to temperate regions with no sea ice. Consequently, Heaton et al. (2020) expressly advise against using their resulting marine radiocarbon calibration curve in regions south of 40°S or north of 50°N due to restricted CO_2 ventilation under varying sea ice conditions over the last 50 ka. Further, they warn against the derivation and application, in a time-invariant manner, of ΔR_R for such higher latitude regions, given that detailed sea-ice histories (and therefore, ventilation) remain poorly constrained and are difficult to model in four dimensions.

Whilst such concerns are valid, the strict application of Marine20 calibration to latitudes south of 50°N in the North Atlantic region excludes extensive areas of mid and high latitude coasts, shelf seas, and ocean that are of vital importance for understanding detailed Late Quaternary climate histories and for which robust chronologies are essential. This includes the entire British Isles, the Baltic, the whole of Scandinavia, Iceland, Greenland, most of Canada, and the Nordic seas. Further, the calculation of a Late Pleistocene to Holocene time-variant ΔR for any specific region requires either a continuous record of paired, contemporaneous marine-terrestrial materials (e.g., accordant raised beach driftwood and whale bone), or an independent chronology on a wide spread of marine ^{14}C dates (e.g., detailed tephrochronology on a marine core) (Alves et al., 2018). In most cases, this is a near impossible task given the scarcity of such materials. The alternative approach of using regional 3D Large Scale Geostrophic Ocean General Circulation models (LSG OGCM) to constrain estimates of ocean ventilation to quantify ΔR_R is also problematic because such simulations only consider single climate scenarios (and thus generate time-invariant ΔR_R), as criticized by Heaton et al. (2020). Developing detailed sea-ice histories based on robust chronologies would be a solution; however, as radiocarbon dating remains the mainstay of such reconstructions, this approach is in danger of becoming circular. Heaton et al. (2020) recommend using local marine reservoir age estimates provided from the LSG OGCM output for calibrating dates that are outside of the Marine20 curve's intended range (i.e., regions north of 40/50°N or south of 40°S). However, simulated reservoir ages, for instance for the Barents Sea region, are highly overestimated by the LSG OGCM (Butzin et al., 2017, 2020), exceeding 1000–1500 years for the last 10 ka – a proposition unsupported by any of the available reservoir ages in the region (e.g., Table 6).

Accepting the technical limitations of calibrating higher-latitude marine ^{14}C dates using Marine20 and *in lieu* of practical alternative approaches we nevertheless recommend the calculation and adoption of regional ΔR calibration terms as a first approximation to aid the direct and applied calibration of marine radiocarbon dates in a practical, user-friendly manner. Indeed, the wide adoption of a standardized common approach to marine ^{14}C calibration is a necessity for meaningful comparisons between marine and terrestrial chronologies derived from radiocarbon and other dating techniques. We reiterate that the ΔR_R terms calculated here apply, in the strictest sense, only for the period and oceanographic conditions for which they were calculated. Nonetheless, in a wider sense, we assert that our ΔR_R values are broadly applicable in the study area for the entire Holocene back to 11.7 cal ka BP due to the relative continuity in oceanographic conditions and sea-ice cover throughout this time (e.g., Rasmussen et al., 2007; Ślubowska-Woldengen et al., 2008; Klitgaard Kristensen et al., 2013; Groot et al., 2014). Notably, extensive regions of the Barents Sea have not been covered by perennial sea ice since the Younger Dryas (SW Barents Sea: Aagaard Sørensen et al., 2010; Hinlopen Strait N of Svalbard: Ślubowska-Woldengen et al., 2008), whilst other areas have been consistently occupied by seasonal, not perennial, sea ice during the Holocene (e.g., Berben et al., 2017; Köseğlu et al., 2018; Pieńkowski et al., 2021). Further, while some changes in Holocene Barents Sea ΔR_R can be expected, the magnitude of such variations is likely small (decadal rather than centennial). For example, only 25 ^{14}C yrs separate our Marine20 ΔR_R terms for northern Norway (−86 ± 39 ^{14}C yrs) and western Svalbard (−61 ± 37 ^{14}C yrs), likely due to differences in sea-ice-moderated ventilation and well within the 2σ error ranges on

both these terms. Whilst we recognize the ongoing challenges associated with ΔR_R in particular and calibration of higher-latitude marine chronologies in general, we, for the above reasons, strongly advocate for the adoption of these newly calculated terms in the Barents Sea region.

5.4. Applicability of ΔR_R

In the strictest sense, our new ΔR_R values are only applicable to the time period covered by the dataset (molluscs: 1857–1937 CE; cetaceans: 1860–1896 CE). However, given that they are based on regionally defined characteristics, we infer their applicability for as long as those broad oceanographic conditions have persisted, i.e., through much of the Holocene (e.g., Klitgaard Kristensen et al., 2013; Groot et al., 2014). Further, we consider our new molluscan ΔR_R terms applicable to other dateable marine carbonate materials commonly found in marine sediment cores (foraminiferal tests, ostracod valves) because of the similarity in diets (phytoplankton, bacteria, organic detritus) and carbon pathways between these organisms (Table 3).

Gaps exist in the coverage of molluscan ΔR_L points (Fig. 1) which complicate the determination of ΔR_R for some parts of the Barents Sea, for example for the central Barents Sea or the area north and east of Svalbard. In these somewhat challenging cases, we recommend assessing the core location in tandem with its modern and palaeo (downcore) oceanographic setting. For example, Holocene radiocarbon dates from a sediment core northeast of Svalbard are likely closer to the western Svalbard ΔR rather than the term from Franz Josef Land due to the continuing influence of Atlantic-source water (Fig. 1). Similarly, for a Holocene core from the central Barents Sea the prevailing oceanography should be identified for the record. For core intervals similar to modern conditions south of the BSAF (identified by suitable proxies), the application of the ΔR_R from northern Norway is likely a robust approach. If reconstructed (or modern) conditions resemble those typical for north of the BSAF, then a northern ΔR_R term should be applied, the appropriate value depending on the core site's proximity to Novaya Zemlya, Franz Josef Land, or Svalbard. In all cases where judgment is used to select the appropriate ΔR_R, a full reasoned justification should be provided. Until new ΔR_L terms become available for the areas that are currently underrepresented or cryptic, we consider this the most robust approach.

It is important to emphasize that our new cetacean ΔR_R values are valid for whales alone and should not be applied to other marine mammals. Work on determining marine-terrestrial offsets for a variety of marine mammals in Arctic Canada (Furze et al., 2014) has demonstrated that ΔR_R varies considerably between animals such as seals, walrus, whales, and polar bears due to different diets and carbon pathways. Until applicable ΔR_R values are determined on the basis of new, specific marine mammal ΔR_L points, we discourage the application of existing molluscan and cetacean ΔR_R terms to other marine mammals.

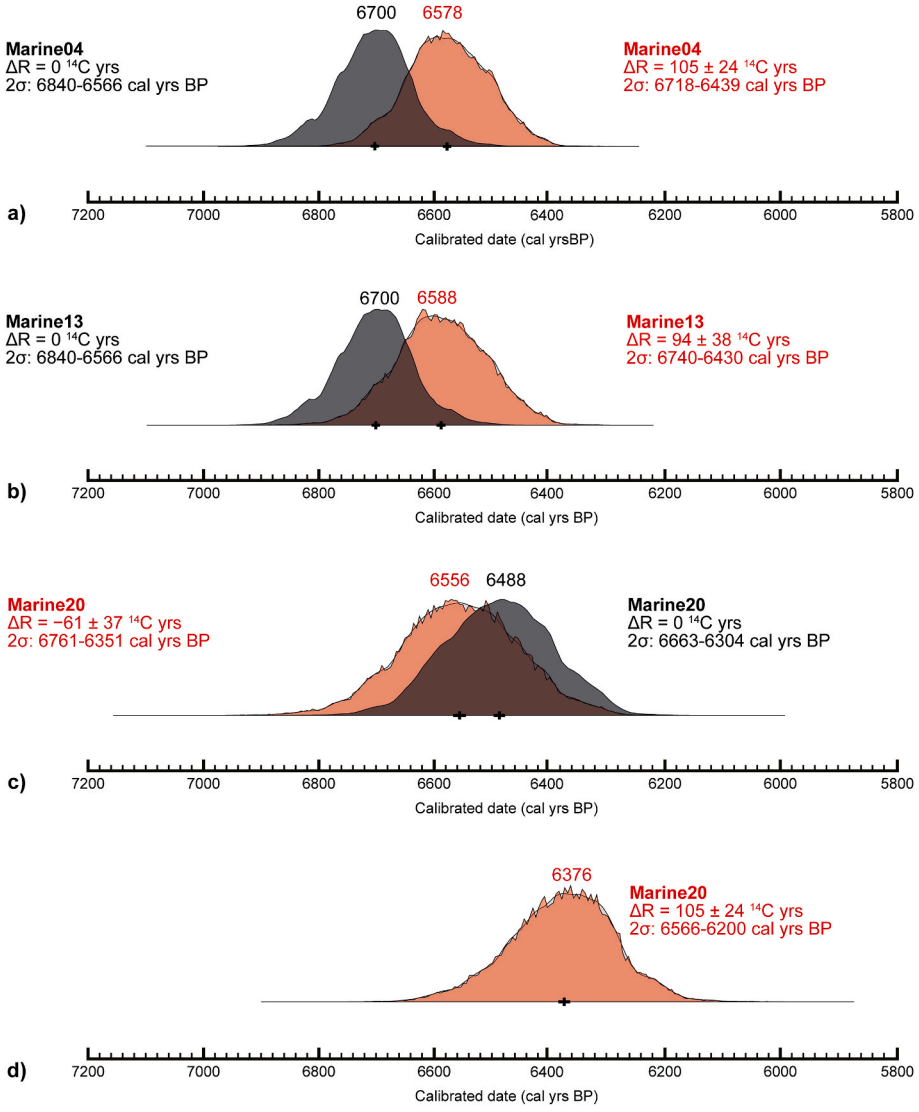

Fig. 3. The importance of calibrating marine radiocarbon dates illustrated by a hypothetical marine date of 6250 ± 50 ^{14}C yrs calibrated in the OxCal program (v.4; Bronk Ramsey, 2009). The median probability date (in cal yrs BP) is above the relevant probability distribution in each case. In a), the date is shown calibrated using Marine04 with $\Delta R = 0$ (i.e., no ΔR) and using a curve-appropriate $\Delta R = 105 \pm 24$ ^{14}C yrs (Bondevik and Gulliksen in Mangerud et al., 2006). In b), the date is calibrated using Marine13 with $\Delta R = 0$ and $\Delta R = 94 \pm 38$ ^{14}C yrs (this study). In c), the date is depicted calibrated in Marine20 with again $\Delta R = 0$ and $\Delta R = -61 \pm 37$ ^{14}C yrs. d) shows the date calibrated in Marine20 with a non-appropriate $\Delta R = 105 \pm 24$ ^{14}C yrs. It becomes apparent that the resulting calibrated age is skewed considerably when either no ΔR or a curve-inappropriate ΔR is used.

With regard to choosing an appropriate cetacean ΔR_R, the identification and separation of baleen and toothed whales are preferable. However, in the case of whale remains found on glacio-isostatically raised shorelines this may not be practically possible. In such cases and given that the ΔR_R terms for toothed and baleen whales are very similar (Table 7), the combined odontocentes-mysticetes term may be used. Lastly, elucidating recent environmental histories occasionally necessitates the use of marine radiocarbon ages beyond the range of calibration curves, i.e., those that are younger than 603 ^{14}C yrs BP (Stuiver et al., 2021). The procedure of how to proceed with such 'young' dates is outlined in Appendix A.

5.5. Importance of appropriate calibration

Calibration, i.e., the conversion of radiocarbon years into calendar-equivalent ages, is essential for meaningful comparisons between marine and terrestrial chronologies, as well as those derived from different dating techniques (Alves et al., 2018). Consequently, calibration and the utilization of ΔR_R in the calibration process is eminently preferable to no calibration, even when uncertainties exist around ΔR_R. However, using the most appropriate ΔR_R term is essential if precision and accuracy are to be maximized, extending beyond considerations regarding oceanographic/geographic, material, and temporal applicability. Importantly, this applies to the matching of ΔR_R terms with the marine calibration curve with which they were calculated, such that ΔR_R calculated from one iteration of the marine calibration curve should not be applied when calibrating with a different curve. For example, the molluscan ΔR_R terms calculated for Svalbard and the Barents Sea by Bondevik and Gulliksen (in Mangerud et al., 2006) were determined from Marine04 (Reimer et al., 2004), and are only applicable to calibrations using that curve. Thus, they should not be used in conjunction with any earlier or later curve (e.g., Marine13); this consideration is particularly important when using Marine20 where the global average marine reservoir age (R) has increased substantially compared to earlier curves (Heaton et al., 2020).

The importance of calibrating marine dates for assuring accuracy is demonstrated in Fig. 3 using a hypothetical marine radiocarbon date (6250 ± 50 ^{14}C yrs) and the Marine04, Marine13, and Marine20 calibration curves. As can be seen in Fig. 3a–d, calibration with no ΔR_R results in multi-decadal to centennial-scale discrepancies with calibration including the appropriate ΔR_R value. Further, calibrating with a mismatched ΔR_R term (calculated from one marine calibration curve but applied to another) also can skew the calibrated age by several hundred years. For example (Figs. 3d), 6250 ± 50 ^{14}C yrs calibrated with Marine20 but using the Bondevik and Gulliksen (in Mangerud et al., 2006) ΔR_R value of 105 ± 24 ^{14}C yrs derived from Marine04 gives a calibrated median probability age 180 cal yrs younger than when calibrated with the appropriate Marine20-derived ΔR_R (this study; Fig. 3c). These examples demonstrate both the necessity of calibrating marine dates using ΔR_R terms and the need to apply calibration curve-appropriate ΔR_R values. Using a ΔR_R of zero due to concerns around changing ΔR_R terms across different marine calibration curve iterations or due to the inconvenience of having to re-calibrate legacy dates is to be expressly avoided. Thus, previously published marine ^{14}C dates should, strictly speaking, be re-calibrated. This is especially important when using Marine20 where R (the global average marine reservoir age) is approximately 1.5 times larger than Marine13.

Furthermore, when (re)calibrating legacy ages it is important to check that marine dates were normalized to the terrestrial standard of $\delta^{13}C = -25‰$ (Stuiver and Polach, 1977), i.e., a "conventional radiocarbon age", given that some early (pre 1990s) marine ages were normalized to $\delta^{13}C = 0‰$. Unnormalized marine ages can be easily normalized by increasing the date by 406.76 ^{14}C yrs prior to calibration (Coulthard et al., 2010). Legacy ages should also be corrected for δ^{13}C fractionation if not previously treated. Where measured δ^{13}C values are available, the new corrected age can easily be calculated (Stuiver and Polach, 1977; Donahue et al., 1990; Reimer et al., 2004) using a spreadsheet available at http://intcal.qub.ac.uk/calib/fractionation.html. If no measured δ^{13}C values are available with which to correct for fractionation, a pooled average value can be calculated from known measured molluscs from that region to derive an approximate δ^{13}C correction term and its 1 standard deviation error (Coulthard et al., 2010). Lastly, we caution against cherry picking ΔR values from online marine reservoir databases such as ^{14}Chrono (http://calib.org/marine/). Whilst it is entirely possible to derive valid ΔR_R terms from such databases, their use requires detailed knowledge of the area's oceanography coupled with a nuanced understanding of the importance different materials (i.e., different organisms, feeding strategies, and carbon pathways) play in influencing observed marine reservoir offsets.

6. Conclusions and recommendations

Based on the derivation of molluscan and whale-based ΔR_R values, the following conclusions and recommendations are made:

- Molluscan-based ΔR_R terms are derived for four broad oceanographic settings prevalent in the Barents Sea; recommended values are as follows: western Svalbard (including Bjørnøya), −61 ± 37 ^{14}C yrs (Marine20) and 94 ± 38 ^{14}C yrs (Marine13); Franz Josef Land, −277 ± 57 ^{14}C yrs (Marine20) and −122 ± 38 ^{14}C yrs (Marine13); Novaya Zemlya, −156 ± 73 ^{14}C yrs (Marine20) and 0 ± 76 ^{14}C yrs (Marine13); northern Norway, −86 ± 39 ^{14}C yrs (Marine20) and 74 ± 24 ^{14}C yrs (Marine13). These values are considered applicable to other marine carbonate materials such as foraminifera and ostracods.
- Recommended cetacean-based ΔR_R terms are as follows: mysticetes (baleen whales), −158 ± 43 ^{14}C yrs (Marine20), 8 ± 41 ^{14}C yrs (Marine13); odontocetes (toothed whales), −161 ± 41 ^{14}C yrs (Marine20), 1 ± 41 ^{14}C yrs (Marine13); combined baleen and toothed whales, −160 ± 41 ^{14}C yrs (Marine20), 4 ± 49 ^{14}C yrs (Marine13). In cases where the identification and separation of baleen and toothed whales is impossible or impractical the combined odontocentes-mysticetes ΔR_R term may be used. However, we explicitly discourage the application of existing cetacean ΔR_R terms to other marine mammals.
- More ΔR_L datapoints for both molluscs and cetaceans would improve the accuracy and precision of ΔR_R.
- We recommend using the latest iteration of the marine calibration curve, Marine20, which seems to better capture the time-variant nature of R compared to Marine13.
- Using the most appropriate (i.e., calibration-curve specific) ΔR_R term in the calibration process is essential if precision and accuracy are to be maximized, extending beyond considerations regarding oceanographic/geographic, material, and temporal applicability.
- Our new ΔR_R values are applicable for as long as those broad oceanographic conditions (circulation and ventilation) have persisted, i.e., through the Holocene.

Funding

This work is a contribution to the Nansen Legacy Project, funded by the Norwegian Research Council (project 276730).

Data availability

All data used and generated in this study are presented in Tables 1, 2,

and 5-7.

Declaration of competing interest

The authors declare that they have no known competing financial interests or personal relationships that could have appeared to influence the work reported in this paper.

Acknowledgments

We thank the Nansen Legacy Project's Palaeo-Subtask group for fruitful discussion surrounding ΔR during the 2020 Age-Models Workshop. Stein Bondevik is thanked for feedback on a draft of this paper. We thank the anonymous reviewers for their constructive comments, and the editor for the handling of this manuscript.

Appendix A

Calibration of 'modern' ^{14}C dates

Marine radiocarbon ages beyond the range of calibration curves (i.e., those younger than 603 ^{14}C yrs BP; Stuiver et al., 2021) can be calibrated to calendar-equivalent ages by using the procedure outlined by Reimer et al. (2004). First, the machine age of the sample can be corrected by subtracting both the global reservoir age at the last year before bomb testing (1955) and the relevant ΔR, as per Equation (A.1). The standard deviation of the resulting '^{14}C age' can be calculated by first determining the errors of the pre-bomb (1955) and the relevant ΔR (Equation (A.2)), and then subsequently using this term with the standard deviation of the machine age (Equation (A.3)).

$$^{14}C\ age = Machine\ age - (R_{AD\ 1955} + \Delta R) \quad \text{(A.1)}$$

(after Reimer et al., 2004)

$$Stdev_{R+\Delta R} = \sqrt{\left(Stdev^{\,2}_{R\ AD\ 1955} + Stdev^{\,2}_{\Delta R}\right)} \quad \text{(A.2)}$$

(after Reimer et al., 2004)

$$Stdev_{14C\ age} = \sqrt{\left(Stdev^{\,2}_{Machine\ age} + Stdev^{\,2}_{R+\Delta R}\right)} \quad \text{(A.3)}$$

(after Reimer et al., 2004).

The resulting '^{14}C age' (Equation (A.1)) and its uncertainty (Equation (A.3)) can be used to calculate fraction modern ($F^{14}C$) in the CaliBomb program (http://calib.org/CALIBomb/). In turn, the resulting $F^{14}C$ and its uncertainty can then be calibrated into yrs AD/BC in CaliBomb (Reimer et al., 2004) using the relevant pre-bomb calibration dataset in conjunction with the appropriate post-bomb calibration data (Northern Hemisphere dataset NHZ1 in the case of the Barents Sea; Hua and Barbetti, 2004).

References

Aguilar, A., García-Vernet, R., 2018. Fin whale: Balaenoptera physalus. In: Würsig, B., Thewissen, J.G.M., Kovacs, K.M. (Eds.), Encyclopedia of Marine Mammals, third ed. Academic Press, pp. 368–371.

Alves, E.Q., Macario, K., Ascough, P., Bronk Ramsey, C., 2018. The worldwide marine radiocarbon reservoir effect: definitions, mechanisms, and prospects. Rev. Geophys. 56, 278–305.

Aagaard-Sørensen, S., Husum, K., Hald, M., Knies, J., 2010. Paleoceanographic development in the SW Barents Sea during the LateWeichselian–early Holocene transition. Quat. Sci. Rev. 29, 1–15.

Bannister, J.L., 2018. Baleen whales (mysticeti). In: Würsig, B., Thewissen, J.G.M., Kovacs, K.M. (Eds.), Encyclopedia of Marine Mammals, third ed. Academic Press, pp. 62–69.

Berben, S.M.P., Husum, K., Navarro-Rodriguez, A., Belt, S.T., Aagaard-Sørensen, S., 2017. Semi-quantitative reconstruction of early to late Holocene spring and summer sea ice conditions in the northern Barents Sea. J. Quaternary Sci. 32, 587–603. https://doi.org/10.1002/jqs.2953.

Beszczynska-Möller, A., Woodgate, R.A., Lee, C., Melling, H., Karcher, M., 2011. A synthesis of exchanges through the main oceanic gateways to the Arctic Ocean. Oceanography 24, 82–99.

Bevington, P.R., Robinson, D.K., 2002. Data Reduction and Error Analysis for the Physical Sciences, third ed. McGraw Hill, p. 320.

Boltunov, A.N., Belikov, S.E., 2002. Belugas (*Delphinapterus leucas*) of the Barents, Kara and laptev seas. NAMMCO Scientific Publications 4, 149–168.

Bronk Ramsey, C., 2009. Bayesian analysis of radiocarbon dates. Radiocarbon 51, 337–360. https://doi.org/10.1017/S0033822200033865.

Butzin, M., Köhler, P., Heaton, T.J., Lohmann, G., 2020. A short note on marine reservoir age simulations used in IntCal20. Radiocarbon 62. https://doi.org/10.1017/RDC.2020.9.

Butzin, M., Köhler, P., Lohmann, G., 2017. Marine radiocarbon reservoir age simulations for the past 50,000 years. Geophys. Res. Lett. 44, 8473–8480. https://doi.org/10.1002/2017GL074688.

Cavalieri, D.J., Parkinson, C.L., 2012. Arctic sea ice variability and trends, 1979–2010. Cryosphere 6, 881–889.

Cipriano, F., 2018. Atlantic white-sided dolphin: lagenorhynchus acutus. In: Würsig, B., Thewissen, J.G.M., Kovacs, K.M. (Eds.), Encyclopedia of Marine Mammals, third ed. Academic Press, pp. 42–44.

Clapham, P.J., 2018. Humpback whale: megaptera novaeangliae. In: Würsig, B., Thewissen, J.G.M., Kovacs, K.M. (Eds.), Encyclopedia of Marine Mammals, third ed. Academic Press, pp. 489–492.

Comiso, J.C., Hall, D.K., 2014. Climate trends in the Arctic as observed from space. WIREs Clim. Change 5, 389–409.

Coulthard, R.D., Furze, M.F.A., Pieńkowski, A.J., Nixon, F.C., England, J.H., 2010. New marine ΔR values for Arctic Canada. Quat. Geochronol. 5, 419–434.

Divine, D.V., Dick, C., 2006. Historical variability of sea ice edge position in the Nordic Seas. J. Geophys. Res. C Oceans Atmos. C01001. https://doi.org/10.1029/2004JC002851.

Donahue, D.J., Linick, T.W., Dull, A.J.T., 1990. Isotope-ratio and background corrections for accelerator mass spectrometry radiocarbon measurements. Radiocarbon 32, 135–142.

Druffel, E.R.M., 1997. Pulses of rapid ventilation in the North Atlantic surface ocean during the past century. Science 275, 1454–1457.

Dyke, A.S., Andrews, J.T., Clark, P.U., England, J.H., Miller, G.H., Shaw, J., Veillette, J. J., 2002. The Laurentide and Innuitian ice sheets during the last glacial maximum. Quat. Sci. Rev. 21, 9–31.

Dyke, A.S., McNeely, R., Southon, J., Andrews, J.T., Peltier, W.R., Clague, J.J., England, J.H., Gagnon, J.-M., Baldinger, A., 2003. Preliminary Assessment of Canadian Marine Reservoir Ages. CANQUA-CCRG 2003 Halifax, Program and Abstracts, p. A23.

Eiríksson, J., Larsen, G., Knudsen, K.L., Heinemeier, J., Símonarson, L.A., 2004. Marine reservoir age variability and water mass distribution in the Iceland Sea. Quat. Sci. Rev. 23, 2247–2268.

Eiríksson, J., Knudsen, K.L., Larsen, G., Olsen, J., Heinemeier, J., Bartels-Jónsdóttir, H.B., Jiang, H., Ran, L., Símonarson, L.A., 2011. Coupling of palaeoceanographic shifts and changes in marine reservoir ages off North Iceland through the last millennium. Palaeogeogr. Palaeoclimatol. Palaeoecol. 302, 95–108.

Elverhøi, A., Dowdeswell, J.A., Funder, S., Mangerud, J., Stein, R., 1998. Glacial and oceanic history of the polar North atlantic margins: an overview. Quat. Sci. Rev. 17, 1–10.

England, J.H., Furze, M.F.A., Doupé, J.P., 2009. Revision of the NW laurentide ice sheet: implications for paleoclimate, thenortheast extremity of beringia, and Arctic ocean sedimentation. Quat. Sci. Rev. 28, 1573–1596.

England, J., Dyke, A.S., Coulthard, R.D., McNeely, R., Aitken, A., 2013. The exaggerated radiocarbon age of deposit-feeding molluscs in calcareous environments. Boreas 42, 362–373.

Farnsworth, W.R., Allaart, L., Ingólfsson, Ó., Alexanderson, H., Forwick, M., Noormets, R., Retelle, M., Schomacker, A., 2020. Holocene glacial history of Svalbard: status, perspectives and challenges. Earth Sci. Rev. 208, 103249. https://doi.org/10.1016/j.earscirev.2020.103249.

Ford, J.K.B., 2018. Killer whale: *Orcinus orca*. In: Würsig, B., Thewissen, J.G.M., Kovacs, K.M. (Eds.), Encyclopedia of Marine Mammals, third ed. Academic Press, pp. 531–537.

Forman, S.L., 1990. Post-glacial relative sea-level history of northwestern Spitsbergen, Svalbard. Geol. Soc. Am. Bull. 102, 1580–1590.

Forman, S.L., Polyak, L., 1997. Radiocarbon content of pre-bomb marine mollusks and variations in the ^{14}C reservoir age for coastal areas of the Barents and Kara seas. Geophys. Res. Lett. 24, 885–888.

Forman, S.L., Lubinski, D.J., Ingólfsson, Ó., Zeeberg, J.J., Snyder, J.A., Siegert, M.J., Matishov, G.G., 2004. A review of postglacial emergence on svalbard, Franz Josef land and Novaya Zemlya, northern eurasia. Quat. Sci. Rev. 23, 1391–1434.

Furze, M.F.A., Pieńkowski, A.J., Coulthard, R.D., 2014. New cetacean ΔR values for Arctic North America and their implications for marine-mammal-based palaeoenvironmental reconstructions. Quat. Sci. Rev. 91, 218–241.

Gammelsrød, T., Leikvin, Ø., Lien, V., Budgell, W.P., Loeng, H., Maslowski, W., 2009. Mass and heat transports in the NE Barents Sea: observations and models. J. Mar. Syst. 75, 56–69.

Groot, D.E., Aagaard-Sørensen, S., Husum, K., 2014. Reconstruction of atlantic water variability during the Holocene in the western Barents Sea. Clim. Past 10, 51–62.

Hacquebord, L., 1999. The hunting of the Greenland right whale in Svalbard, interaction with climate and its impact on the marine ecosystem. Polar Res. 18, 375–382.

Hacquebord, L., 2001. Three Centuries of whaling and walrus hunting in Svalbard and its impact on the Arctic ecosystem. Environ. Hist. 7, 169–185.

Hacquebord, L., Avango, D., 2016. Industrial heritage sites in spitsbergen (svalbard), south Georgia and the antarctic peninsula: sources of historical information. Polar Science 10, 433–440.

Heaton, T.J., Köhler, P., Butzin, M., Bard, E., Reimer, R.W., Austin, W.E.N., Ramsey, C.B., Grootes, P.M., Hughen, K.A., Kromer, B., Reimer, P.J., Adkins, J., Burke, A., Cook, M. S., Olsen, J., Skinner, L.C., 2020. Marine20 – the marine radiocarbon age calibration curve (0-55,000 cal BP). Radiocarbon 62, 779–820.

Hooker, S.K., 2018. Toothed whales (odontoceti). In: Würsig, B., Thewissen, J.G.M., Kovacs, K.M. (Eds.), Encyclopedia of Marine Mammals, third ed. Academic Press, pp. 1004–1010.

Horwood, J., 2018. Sei whale: *Balaenoptera borealis*. In: Würsig, B., Thewissen, J.G.M., Kovacs, K.M. (Eds.), Encyclopedia of Marine Mammals, third ed. Academic Press, pp. 845–847.

Hua, Q., Barbetti, M., 2004. Review of tropospheric bomb ^{14}C data for carbon cycle modeling and age calibration purposes. Radiocarbon 46, 1273–1298.

Hua, Q., Woodroffe, C.D., Smithers, S.G., Barbetti, M., Fink, D., 2005. Radiocarbon in corals from the cocos (keeling) islands and implications for Indian ocean circulations. Geophys. Res. Lett. 32, L21602. https://doi.org/10.1029/2005GL023882.

Hughen, K., Lehman, S., Southon, J., Overpeck, J., Marchal, O., Herring, C., Turnbull, J., 2004. ^{14}C activity and global carbon cycle changes over the past 50,000 years. Science 303, 202–207.

Ingvaldsen, R., Loeng, H., 2009. Physical oceanography. In: Sakshaug, E., Johnsen, G., Kovacs, K. (Eds.), Ecosystem Barents Sea. Tapir Academic Press, Trondheim, Norway, pp. 33–64.

Jørgensen, R., 2005. Archaeology on svalbard: past, present and future. Acta Boreal. 22, 49–61.

Kenney, R.D., 2009. Right whale: *Eubalaena glacialis, E. japonica*, and *E. australis*. In: Perrin, W.F., Würsig, B., Thewissen, J.G.M. (Eds.), Encyclopedia of Marine Mammals, second ed. Academic Press, pp. 962–972.

Kinze, C.C., 2018. White-beaked dolphin: *Lagenorhynchus albirostris*. In: Würsig, B., Thewissen, J.G.M., Kovacs, K.M. (Eds.), Encyclopedia of Marine Mammals, third ed. Academic Press, pp. 1077–1079.

Klitgaard Kristensen, D., Rasmussen, T.L., Koç, N., 2013. Palaeoceanographic changes in the northern Barents Sea during the last 16 000 years – new constraints on the last deglaciation of the Svalbard–Barents Sea ice sheet. Boreas 42, 798–813.

Kovacs, K.M., Gjertz, I., Lydersen, C., 2004. Marine Mammals of Svalbard. Norwegian Polar Institute, Tromsø, Norway, p. 64.

Köseoğlu, D., Belt, S.T., Smik, L., Yao, H., Panieri, G., Knies, J., 2018. Complementary biomarker-based methods for characterising Arctic sea ice conditions: a case study comparison between multivariate analysis and the PIP_{25} index. Geochem. Cosmochim. Acta 222, 406–420.

Kwok, R., 2009. Outflow of Arctic ocean sea ice into the Greenland and Barents seas: 1979-2007. J. Clim. 22, 2438–2457.

Langer, P.D., 1978. Some Aspects of the Biology of Three Northwestern Atlantic Chitons: *Tonicella rubra, Tonicella marmorea*, and *Ischnochiton albus* (Mollusca: Polyplacophora). University of New Hampshire, Durham, p. 205 unpublished PhD thesis.

Loeng, H., 1991. Features of the physical oceanographic conditions of the Barents Sea. Polar Res. 10, 5–18.

Mangerud, J., Bondevik, S., Gulliksen, S., Hufthammer, A.K., Høisæter, T., 2006. Marine ^{14}C reservoir ages for 19th century whales and molluscs from the North Atlantic. Quat. Sci. Rev. 25, 3228–3245.

Mangerud, J., Gulliksen, S., 1975. Apparent radiocarbon ages of recent marine shells from Norway, Spitsbergen, and Arctic Canada. Quat. Res. 5, 263–273.

McConnaughey, T.A., Gillikin, D.P., 2008. Carbon isotopes in mollusk shell carbonates. Geo Mar. Lett. 28, 287–299.

Olson, P.A., 2018. Pilot whales: *Globicephala melas* and *G. macrorhynchus*. In: Würsig, B., Thewissen, J.G.M., Kovacs, K.M. (Eds.), Encyclopedia of Marine Mammals, third ed. Academic Press, pp. 701–705.

Ozhigin, V.K., Trofimov, A.G., Ivshin, V.A., 2000. The eastern basin water and currents in the Barents Sea. ICES Annual Science Conference 2000, 19.

Paar, M., Lebreton, B., Graeve, M., Greenacre, M., Asmus, R., Asmus, H., 2019. Food sources of macrozoobenthos in an Arctic kelp belt: trophic relationships revealed by stable isotope and fatty acid analyses. Mar. Ecol. Prog. Ser. 615, 31–49.

Parsons, A.R., Bourke, R.H., Muench, R.D., Chiu, C.-S., Lynch, J.F., Miller, J.H., Plueddemann, A.J., Pawlowicz, R., 1996. The Barents Sea polar front in summer. J. Geophys. Res. 101, 14201–14221.

Peacock, J.D., 1993. Late Quaternary marine Mollusca as palaeoenvironmental proxies: a complication and assessment of basic numerical data for NE Atlantic species found in shallow water. Quat. Sci. Rev. 12, 263–275.

Perrin, W.F., Mallette, S.D., Brownell Jr., R.L., 2018. Minke whales: *Balaenoptera acutorostrata* and *B. bonaerensis*. In: Würsig, B., Thewissen, J.G.M., Kovacs, K.M. (Eds.), Encyclopedia of Marine Mammals, third ed. Academic Press, pp. 608–613.

Petchey, F., Anderson, A., Zondervan, A., Ulm, S., Hogg, A., 2008. New marine ΔR values for the South Pacific subtropical gyre region. Radiocarbon 50, 373–397.

Pfirman, S.L., Bauch, D., Gammelsrød, T., 1994. The northern Barents Sea: water mass distribution and modification. In: Johannessen, O.M., Muench, R.D., Overland, J.E. (Eds.), The Polar Oceans and Their Role in Shaping the Global Environment: the Nansen Centennial Volume. American Geophysical Union, Washington DC, pp. 77–94.

Pieńkowski, A.J., Husum, K., Belt, S.T., Ninneman, U., Köseoğlu, D., Divine, D.V., Smik, L., Knies, J., Hogan, K., Noormets, R., 2021. Seasonal sea ice persists through the Holocene Thermal Maximum at 80°N. Commun. Earth Environ. 2, 124. https://doi.org/10.1038/s43247-021-00191-x.

Rasmussen, T.L., Thomsen, E., Ślubowska, M.A., Jessen, S., Solheim, A., Koç, N., 2007. Paleoceanographic evolution of the SW Svalbard margin (76°N) since 20,000 ^{14}C yr BP. Quat. Res. 67, 100–114.

Reimer, P.J., Brown, T.A., Reimer, R.W., 2004. Discussion: reporting and calibration of post-bomb ^{14}C data. Radiocarbon 46, 1299–1304.

Reimer, P.J., Baillie, M.G.L., Bard, E., Bayliss, A., Beck, J.W., Blackwell, P.G., Ramsey, C. B., Buck, C.E., Burr, G.S., Edwards, R.L., Friedrich, H.M., Grootes, P.M., Guilderson, T.P., Hajdas, I., Heaton, T.J., Hogg, A.G., Hughen, K.A., Kaiser, K.F., Kromer, B., McCormac, F.G., Manning, S.W., Reimer, R.W., Richards, D.A., Southon, J.R., Talamo, S., Turney, C.S.M., Van Der Plicht, J., Weyhenmeyer, C.E., 2009. IntCal09 and Marine09 radiocarbon age calibration curves, 0-50 000 years cal BP. Radiocarbon 51, 1111–1150.

Reimer, P.J., Bard, E., Bayliss, A., Beck, J.W., Blackwell, P.G., Ramsey, C.B., Buck, C.E., Cheng, H., Edwards, R.L., Friedrich, M., Grootes, P.M., Guilderson, T.P., Haflidason, H., Hajdas, I., Hatté, C., Heaton, T.J., Hoffmann, D.L., Hogg, A.G., Hughen, K.A., Kaiser, K.F., Kromer, B., Manning, S.W., Niu, M., Reimer, R.W., Richards, D.A., Scott, E.M., Southon, J.R., Staff, R.A., Turney, C.S.M., van der Plicht, J., 2013. IntCal13 and Marine13 radiocarbon age calibration curves 0–50,000 Years cal BP. Radiocarbon 55, 1869–1887.

Renner, A.H.H., Sundfjord, A., Janout, M.A., Ingvaldsen, R.B., Beszczynska-Möller, A., Pickart, R.S., Pérez-Hernández, M.D., 2018. Variability and redistribution of heat in the Atlantic Water boundary current north of Svalbard. J. Geophysical Research Oceans 123, 6373–6391.

Schell, D.M., Saupe, S.M., Haubenstock, N., 1989. Bowhead whale (*Balaena mysticetus*) growth and feeding as estimated by δ^{13}C techniques. Mar. Biol. 103, 433–443.

Schlitzer, R., 2020. Ocean Data View. https://odv.awi.de.

Selin, N.I., 2007. Shell form, growth and life of *Astarte arctica* and *A. borealis* (Mollusca: Bivalvia) from the subtidal zone of northeastern Sakhalin. Russ. J. Mar. Biol. 33, 232–237.

Sears, R., Perrin, W.F., 2018. Blue whale *Balaenoptera musculus*. In: Würsig, B., Thewissen, J.G.M., Kovacs, K.M. (Eds.), Encyclopedia of Marine Mammals, third ed. Academic Press, pp. 110–114.

Shumway, S.E., Parsons, J.G. (Eds.), 2006. Scallops: Biology, Ecology and Aquiculture. Elsevier, Amsterdam.

Scourse, J.D., Richardson, C.A., Forsythe, G., Harris, I., Heinemeier, J., Fraser, N.M., Briffa, K.R., Jones, P.D., 2006. First cross-matched floating chronology from the marine fossil record: data from growth lines of the long-lived bivalve mollusc *Arctica islandica*. Holocene 16, 967–974.

Ślubowska-Woldengen, M., Koç, N., Rasmussen, T., Jennings, A.E., 2008. Time-slice reconstructions of ocean circulation changes on the continental shelf in the Nordic and Barents Seas during the last 16,000 cal yr BP. Quat. Sci. Rev. 27, 1476–1492.

Smedsrud, L.H., Esau, I., Ingvaldsen, R.B., Eldevik, T., Haugan, P.M., Li, C., Lien, V.S., Olsen, A., Omar, A.M., Otterå, O.H., Risebrobakken, B., Sando, A.B., Semenov, V.A., Sorokina, S.A., 2013. The role of the Barents Sea in the arctic climate system. Rev. Geophys. 51, 415–449.

Smith, B.D., Cabot, E.L., Foreman, R.E., 1985. Seaweed detritus versus benthic diatoms as important food resources for two dominant subtidal gastropods. Journal of Experimental Marine Biology 92, 143–156.

Sundfjord, A., Assmann, K.M., Lundesgaard, Ø., Renner, A.H.H., Lind, S., Ingvaldsen, R. B., 2020. Suggested water mass definitions for the central and northern Barents Sea, and the adjacent Nansen Basin: workshop report. The Nansen Legacy Report Series 8/2020. https://doi.org/10.7557/nlrs.5707.

Storrie, L., Lydersen, C., Andersen, M., Wynn, R.B., Kovacs, K.M., 2018. Determining the species assemblage and habitat use of cetaceans in the Svalbard Archipelago, based on observations from 2002 to 2014. Polar Res. 37, 1–22.

Stuiver, M., Braziunas, T., 1985. Compilation of isotopic dates from Antarctica. Radiocarbon 27 (2A), 117–304.

Stuiver, M., Polach, H.A., 1977. Reporting of ^{14}C data. Radiocarbon 19, 355–363.

Stuiver, M., Pearson, G.W., Braziunas, T., 1986. Radiocarbon age calibration of marine samples back to 9000 cal yr BP. Radiocarbon 28 (2B), 980–1021.

Stuiver, M., Reimer, P.J., Reimer, R.W., CALIB 8.2 [WWW program], 2021. http://calib.org, 13, 4.

Ulm, S., 2006. Australian marine reservoir effects: a guide to ΔR values. Aust. Archaeol. 63, 57–60.

Vinje, T., 2001. Anomalies and trends of sea ice extent and atmospheric circulation in the Nordic Seas during the period 1864-1998. J. Clim. 14, 255–267.

Ward, G.K., Wilson, S.R., 1978. Procedures for comparing and combining radiocarbon age determinations: a critique. Archaeometry 20, 19–31.

Whitehead, H., 2018. Sperm whale: *Physeter macrocephalus*. In: Würsig, B., Thewissen, J. G.M., Kovacs, K.M. (Eds.), Encyclopedia of Marine Mammals, third ed. Academic Press, pp. 919–925.

Wood, R., 2015. From revolution to convention: the past, present and future of radiocarbon dating. J. Archaeol. Sci. 56, 61–72.

Zotin, A.A., Ozernyuk, N.D., 2004. Growth characteristics of the common mussel *Mytilus edulis* from the White Sea. Biol. Bull. 31, 377–381.